Journal of Earthquake Engineering

ISSN: 1363-2469 (Print) 1559-808X (Online) Journal homepage: www.tandfonline.com/journals/ueqe20

Assessment of Seismic Capacity of Building Envelope Nonstructural Components

Antonio Bonati, Nicola Caterino, Maddalena Cimmino, Orsola Coppola, Alessandra De Angelis, Giuseppe Maddaloni & Antonio Occhiuzzi

To cite this article: Antonio Bonati, Nicola Caterino, Maddalena Cimmino, Orsola Coppola, Alessandra De Angelis, Giuseppe Maddaloni & Antonio Occhiuzzi (2026) Assessment of Seismic Capacity of Building Envelope Nonstructural Components, Journal of Earthquake Engineering, 30:1, 192-227, DOI: 10.1080/13632469.2025.2470328

To link to this article: https://doi.org/10.1080/13632469.2025.2470328

Published online: 10 Mar 2025.

JOURNAL OF EARTHQUAKE ENGINEERING
2026, VOL. 30, NO. 1, 192–227
https://doi.org/10.1080/13632469.2025.2470328

Assessment of Seismic Capacity of Building Envelope Nonstructural Components

Antonio Bonati[a], Nicola Caterino[b,c], Maddalena Cimmino[c], Orsola Coppola[a], Alessandra De Angelis[d], Giuseppe Maddaloni[c,d], and Antonio Occhiuzzi[a,b]

[a]Construction Technologies Institute, National Research Council, Milano, Italy; [b]Department of Engineering, University of Naples "Parthenope", Naples, Italy; [c]Construction Technologies Institute, National Research Council, Napoli, Italy; [d]Department of Engineering, University of Sannio, Benevento, Italy

ABSTRACT
This paper describes an innovative "testing set" for assessing the seismic capacity of building envelopes consisting of a specialized testing equipment and a companion testing protocol. The equipment has been designed for assessing the seismic capacity of either building envelopes or their components, based on a historical review of testing machine for such nonstructural elements. The testing protocol is designed to adapt recent code provisions to building envelopes. The testing set is proposed for both external cladding systems and precast concrete panels' connections. In the latter case, the experimental activity led to an assessment criterium for the connections seismic design.

ARTICLE HISTORY
Received 1 August 2024
Accepted 5 February 2025

KEYWORDS
Non-structural components; external wall claddings; precast concrete panel; connections; seismic assessment methods; dynamic tests; quasi-static tests

1. Introduction

A major shift of attention in the evaluation of seismic behavior from structural to nonstructural components is probably due to the Pacific Earthquake Engineering Research Center Report 2003/05 by Taghavi and Miranda (2003), that first showed that most of the economic losses associated with earthquakes comes from damage to nonstructural components. They also stated that nonstructural components can be categorized as follows:

- interstory-drift sensitive;
- acceleration sensitive;
- interstory-drift sensitive and acceleration sensitive.

Subsequently, many researchers tried to set up analytical frameworks for the evaluation of seismic demand and the assessment of seismic capacity of nonstructural components. The proposals for the evaluation of the seismic demand are substantially based on the definition of floor response spectra for nonstructural components (Huang et al. 2017; Kazantzi, Vamvatsikos, and Miranda 2020; Medina, Sankaranarayanan, and Kingston 2006; Oropeza, Favez, and Lestuzzi 2010). A notable exception is a simplified method to calculate the maximum lateral forces that may be generated by a specified earthquake ground motion on the masses of a nonstructural component attached to a building structure (Villaverde 2006). Also design methodologies based on direct displacement-based seismic design are making their way in the world of nonstructural components (Merino, Perrone, and Filiatrault 2022).

Conversely, the assessment of the seismic capacity was found to be strongly dependent on the type of nonstructural components at hand. For instance, Magliulo et al. (2012) and Pourali et al. (2017) adopted shake table tests for suspended ceilings, Fiorino et al. (2023) adopted quasi-static tests for

CONTACT Orsola Coppola orsola.coppola@itc.cnr.it Construction Technologies Institute, National Research Council, Milano, Italy

lightweight steel drywall façades, Aghababaei et al. (2021) proposed the adoption of terrestrial laser-scanning techniques to document observations during these tests and Wynn et al. (2022) tested both wooden structural and various nonstructural components on the shake table. In the context of seismic capacity of nonstructural components, building envelopes make a special class of construction products. As examples, Bedon et al. (2018) and Bianchi et al. (2024) described how the multi-functional use of façades requires a complex design approach considering many different perspectives for such components.

The different approaches to demand evaluation and capacity assessment are due not only to the categorization as interstory-drift or acceleration sensitive for nonstructural components but also to the different nature of such components compared to classical structural members. The large variety of materials, material combinations, supporting systems and geometries, together with joints completely different from those adopted in concrete and steel structures, makes it difficult to adopt consolidated analytical tools of structural engineering to nonstructural components. Therefore, in a large number of cases the assessment of seismic capacity of nonstructural components needs an experimental approach. This, in turn, yields a need for testing protocols which often borrow the equipment from structural and seismic engineering, but require specific rules in order to obtain significant results (Mulligan, Sullivan, and Dhakal 2020; Zito, D'Angela, et al. 2022; Zito, Nascimbene, et al. 2022).

Seismic capacity of non-structural components must be approached both at ultimate limit states (ULS) and serviceability limit states (SLS). As for building envelopes, in the first case (ULS) breakages can directly result in life hazard if debris falls from the façade to the ground. However, even if safety at ULS is guaranteed, damage to building envelopes can endanger their capability of service in terms of air and water tightness and, in turn, the possibility of operating a building after an earthquake. Therefore, seismic capacity of building envelopes should be assessed both at the ULS and the SLS at corresponding seismic intensity levels (Bianchi and Pampanin 2022).

This paper aims to describe an innovative approach for the assessment of the seismic capacity of building envelopes, where both the testing equipment and the corresponding protocols are specifically designed and realized for these nonstructural components. The specific equipment proposed allows the use of a testing protocol specialized for building envelope components without trading off testing accuracy and significance for the adoption of pre-existing standard testing machines. The proposed equipment and the protocol match perfectly with each other and they are capable to test both acceleration sensitive and interstory-drift sensitive components, to apply quasi-static and dynamic actions and to operate contemporarily both in-plane (IP) and out-of-plane (OOP) directions. The description of the proposed equipment and of the corresponding testing protocol is preceded by an historical excursus on testing machines for façades that greatly helped the authors to understand how to design and to operate the new equipment.

2. Testing Methods for Building Envelopes Against Seismic Loads: An Historical Overview

The seismic behavior of building envelopes remains a topic marked by numerous uncertainties. Since the latter half of the twentieth century, research in this field has advanced, necessitating ongoing experimental efforts to investigate and understand the dynamic behavior and seismic performance of these components. Initially, significant attention was devoted to evaluating the experimental response to in-plane displacements applied statically. Over time, the focus expanded to include out-of-plane response and significant load application rates (dynamic response). Indeed, as said above, Taghavi and Miranda (2003) clarified that non-structural components, in general, may be more sensitive to displacements, accelerations, or a combination of the two. Specifically concerning the building envelope components examined in the present study, Taghavi and Miranda classified masonry walls and windows as drift-sensitive, parapets as acceleration-sensitive, and precast elements as both drift- and acceleration-sensitive. It is worth specifying that the focus of this work is primarily on elements such as cladding and glazing. Indeed, for these elements subsequent studies have shown that, for a proper characterization of the seismic response, it is important to always consider both their vulnerability to in-plane displacements and out-of-plane accelerations.

Here, a historical overview of the methods and systems developed over the past decades to investigate this topic is presented. More frequent reference will be made to glazing systems, for which the earliest laboratory investigations are more remote, initially even focused on the "window" element. However, the investigation methods being discussed are often versatile and suitable for testing different components, provided they serve the same architectural function.

2.1. The Evolution of Testing Machines Over Time

Since the 1960s, several researchers have sought to clarify the issue of seismic capacity assessment by conducting laboratory experiments and assisting leading regulatory bodies in developing guidelines for the field. The earliest experiments known to the authors date back to studies conducted by Bouwkamp and Meehan (Bouwkamp 1960; Bouwkamp and Meehan 1960). They realized pin-connected steel frames of various sizes, ranging from (height x width) 61 × 122 cm to 244 × 122 cm and installed windows with different frame materials (steel, aluminum, wood), glass types, glass-to-frame clearances, and dimensions. The window panels were connected to the hinged steel frame by means of wood members. A horizontal load was applied to the top of the frame, while a spring installed at mid-height was used to maintain the system's equilibrium in any deflected position (Fig. 1).

A number of 33 specimens were tested under static loads mainly to investigate the role of each of the construction details. Additional two tests were performed under cyclic loads and four further specimens against impact loads. They measured the in-plane movements of the glass panel with respect to the frame, those of the overall window panel and the out-of-plane movements of the glass panel. This is a pioneering work, thus highly innovative for its time. The system clearly did not allow for dynamic testing or the application of out-of-plane forces. However, the authors drew some significant conclusions about the ultimate drift of a window panel under the load conditions adopted and its dependency on the above variables.

Thurston and King (1992) performed the last part of a wide BRANZ (Building Research Association of New Zealand) research program about the earthquake behavior of glazing systems. While the earlier work at BRANZ looked at in-plane behavior for single window specimens of 140 × 122 cm and 280 × 122 cm with 6-mm thick glass, Thurston and King focused on a two-way loading (in-plane and out-of-plane) technique, with special attention to portion of glazing near building corners. They tested three full-size generic wall types: a conventional dry-glazed gasketed curtain wall, a unitized structural silicone system, and a combination unitized system comprising structural silicone on two sides of each glass panel with conventional gaskets on the other two sides. Sinusoidal loading was applied in the two horizontal directions to a 3-story glazing wall consisting of four panels at each level, arranged in an L-shape (corner configuration, Fig. 2). The authors found that rotation of the glass within the window system is the largest contributor to the deformation capacity of the system. In essence, this work led to the innovation of testing both in-plane and out-of-plane behavior, although with reference to a very specific facade configuration (corner). Among the added values, the analysis that the authors performed regarding the sensitivity of the response to the load rate.

In the early 1990s, an important multi-year research project on the topic started at the University of Missouri-Rolla (UMR). Deschenes (1991) introduced a specific machine for the in-plane dynamic racking: the curtain wall was racked back and forth in a motion that was parallel to the plane of the façade component. The lower tube was designed to move in its longitudinal direction while the upper tube was restrained from any movement. The lower sliding tube was supported at each end by an assembly of brass rollers that allowed smooth sliding while restraining out-of-plane motion. Lower tube displacement was pushed by a 98 kN hydraulic actuator with a full stroke of 152 mm (±76 mm) using a displacement-control approach. Culp (1993) made an extension of the earlier study conducted by Deschenes et al. (1991), aimed at investigating the out-of-plane behavior also. The UMR machine was modified accordingly to perform this new type of

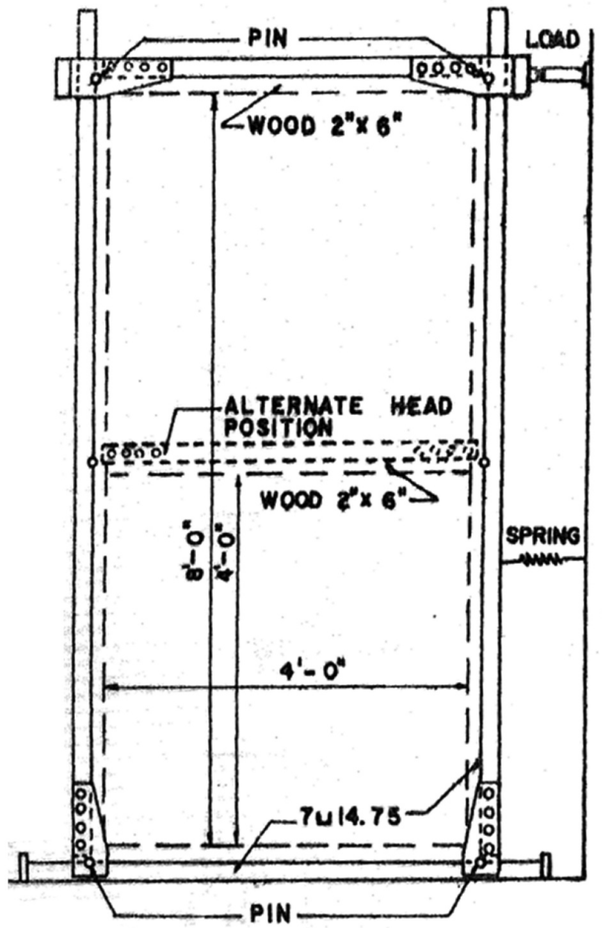

Figure 1. Hinged loading frame suitable for 122 × 122 cm (4′×4′) and 244 × 122 cm (8′×4′) window panels (after Bouwkamp and Meehan 1960).

test. A new roller assembly was designed to enable the axial movement of the hydraulic actuator ram to produce mechanically coupled in-plane and out-of-plane motions of the sliding bottom tube (Fig. 3). The actuator was connected to the sliding tube by a universal-joint, a straight link, and a vertical pin, with rollers that guided the edges of moving angled wedges, yielding an out-of-plane displacement equal to 50% of the in-plane displacement.

In 1995, the facility at UMR was adapted to produce racking motions that approximate the earthquake induced inter-story drifts for typical multistory buildings, for samples up to 4.72 × 3.66 m. As shown in Fig. 4 (R. A. Behr, Belarbi, and Brown 1995), the two tubular steel beams, formally representing the beams of two adjacent stories of a multi-story building, are connected by a pivot arm with fulcrum that makes possible to induce higher drifts than before. Actually, in-plane inter-story drifts were applied to the wall system test assembly by the actuator at the bottom that causes the bottom beam to slide at the same time making the top beam to displace an equal distance in the opposite direction, thanks to the pivot arm (R. Behr and Belarbi 1996). The system was capable of reproducing 76 mm in-plane racking amplitudes at a frequency of 1 hz, with higher frequencies achievable at lower displacement magnitude.

In subsequent years, the UMR testing machine has been adapted to host different kinds of specimens and experimental campaigns. Fig. 5 shows the adaptation made by Brueggeman et al. (2000) to

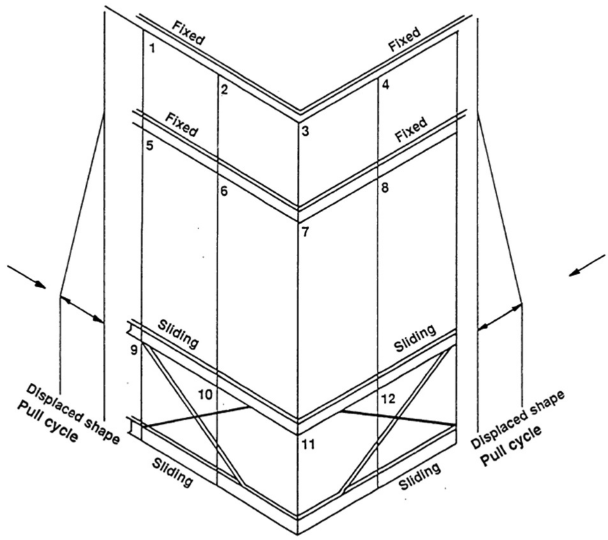

Figure 2. Schematic representation of the test set-up for glazing in a corner configuration (after Thurston and King 1992).

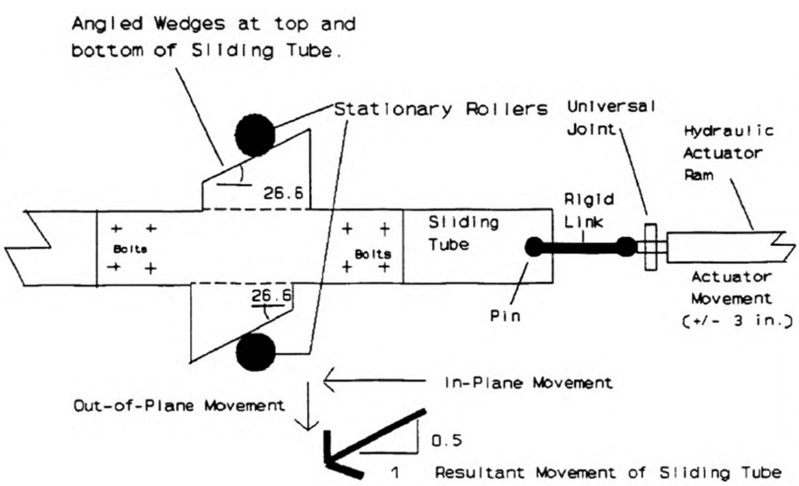

Figure 3. A detail (plan view) of the UMR test facility as modified by Culp (1993) for combined in-plane and out-of-plane motion.

test Earthquake-Isolated Curtain Wall Systems (EICWSs). In this case, the upper and lower steel beams were fixed, while a middle steel tube was installed and allowed to slide, with movements controlled by the actuator. Actually, for the EICWS specimens there was the need to support the vertical mullions at only one-story level of the ideal primary building structure, mainly to investigate the effectiveness of the decoupler joints for the seismic isolation of the curtain wall.

In practice, with the facility at UMR, seismic testing of facade components made significant progress in reproducing signals sufficiently large in displacement, yet constrained in-plane and with low-to-medium frequency. In the last decade, a second generation of testing machines for façades and, more generally, for building envelopes has been developed to overcome these limitations as well as to include environmental and comfort aspects in the experimental tests, both pre- and post-earthquake. One of the most advanced machines at the moment is the one installed at the Institute for Construction Technologies (ITC) of the Italian National Research Council (CNR) in San Giuliano

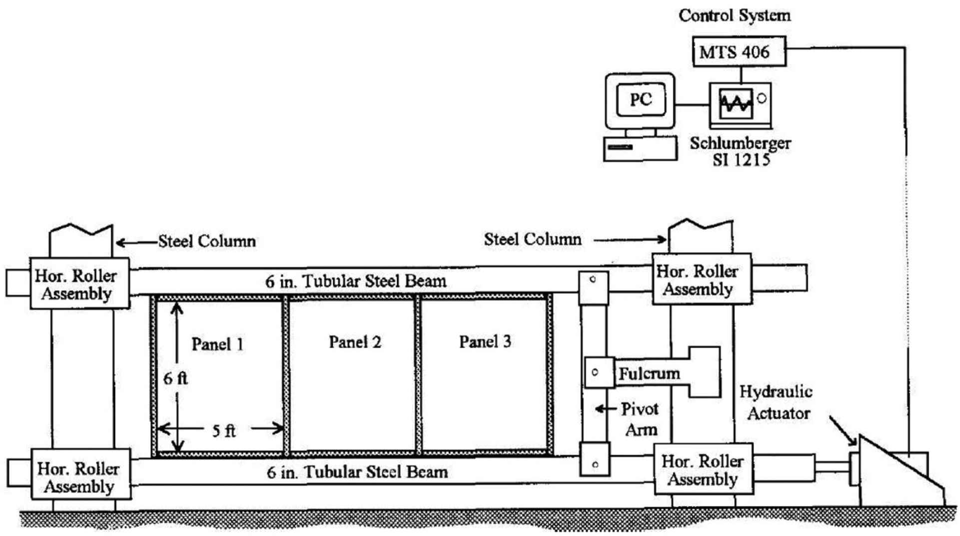

Figure 4. Schematic of the UMR storefront wall system test assembly (after R. A. Behr, Belarbi, and Brown 1995).

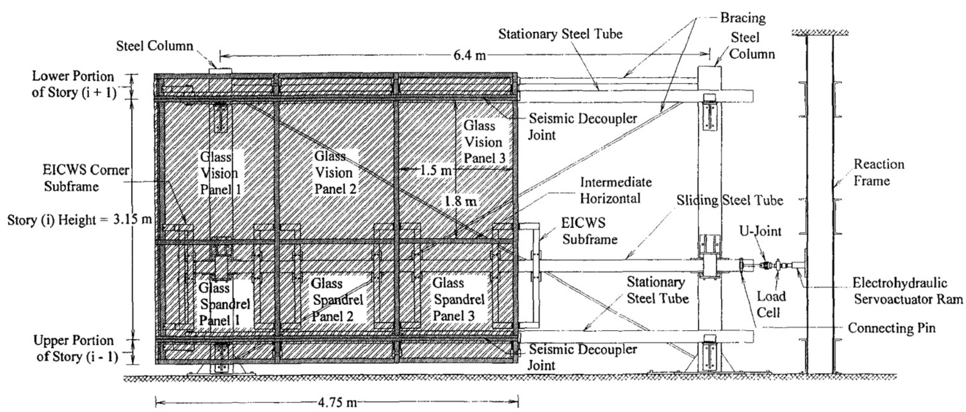

Figure 5. The UMR testing machine adapted by Brueggeman et al. (2000) to test EICWSs.

Milanese (Milan, Italy). The facility, able to test the primary performances expected from a façade system in terms of resistance against wind pressure, static and dynamic water-tightness and air leakage, was improved to reproduce also in-plane and out-of-plane static and dynamic seismic loads. This machine is described in detail in the following sections.

2.2. The Evolution of the Testing Protocols Over Time

The most significant evolutions that the testing protocols have undergone over time are described in the following. As said above, Bouwkamp and Meehan (Bouwkamp 1960; Bouwkamp and Meehan 1960) conducted the first experiments on building envelope components (glazing systems) using static loads, monotonic or cyclic, up to ultimate condition of the specimen and by imposing in-plane and out-of-plane movements. Culp, much later (Culp 1993), made an initial attempt to formalize seismic input through the definition of a rather detailed protocol. To evaluate the dynamic performance of curtain wall glass elements, he proposed a test consisting of two phases (Fig. 6). The first one (frequency not higher than 1 hz) approximated the inter-story drifts and associated frequencies that

TABLE I. TEST SEQUENCES FOR DYNAMIC IN-PLANE/ OUT-OF-PLANE RACKING TESTS

PHASE I

	In-Plane Amplitude (in.)	Out-of-Plane Amplitude (in.)
1 HZ — **5 CYCLES PER AMPLITUDE**		
	0.19	0.10
	0.39	0.20
	0.59	0.30
	0.79	0.40
	0.98	0.49
	1.18	0.59
	1.38	0.69
	1.57	0.79
0.5 HZ — **5 CYCLES PER AMPLITUDE**		
	1.77	0.89
	1.97	0.99
	2.16	1.08
	2.36	1.18
	2.56	1.28
	2.75	1.38
	2.95	1.48

PHASE II (Repeated 10 times)

60 CYCLES PER AMPLITUDE

Frequency	In-Plane Amplitude (in.)	Out-of-Plane Amplitude (in.)
4 HZ	0.40	0.20
3 HZ	0.60	0.30
2 HZ	1.00	0.50
1 HZ	2.50	1.25

(1 in. = 25.4 mm)

Figure 6. Testing protocol for curtain wall glass elements according to Culp (1993).

would be present in the response of a typical 15-story steel frame structure during a moderate earthquake. The second one (frequency up to 4 hz), which was conducted immediately after the first, included a more severe combination of amplitudes, frequencies, and number of cycles than those of the first step, so that the post breakage fallout behavior of various glass types could be observed with greater evidence. The maximum amplitude/frequency combinations were limited due to the physical limits of the UMR hydraulic actuator. The test sequences for both phases I and II are outlined in (Fig. 6).

Pantelides and Behr (1994) conducted in-plane tests in displacement control with a modified input type compared to Culp (1993). The new input was aimed at overcoming the physical limits of the mechanical equipment available at the time. A third test sequence was added, that began with the curtain wall test section at an initial racked displacement of 76 mm (Fig. 7). This pre-racking allowed a maximum 152 mm racking amplitude when the actuator reached its maximum 76 mm positive stroke and caused the test frame to be in a plumb position at the minimum stroke.

To develop more representative laboratory loading histories and address both serviceability and ultimate limit states, R. A. Behr, Belarbi, and Brown (1995) evaluated the seismic performance of a commonly used storefront wall system using as loading history a simplified version of the response analyzed from an existing storefront building subjected to the ground motion accelerogram of the May 18, 1940, El Centro earthquake. This simplified response consisted of 65 sinusoidal cycles with variable amplitudes and a constant frequency of 0.8 hz, including a maximum racking amplitude of ±43 mm. This loading history, deemed representative of a maximum probable earthquake event, was used to

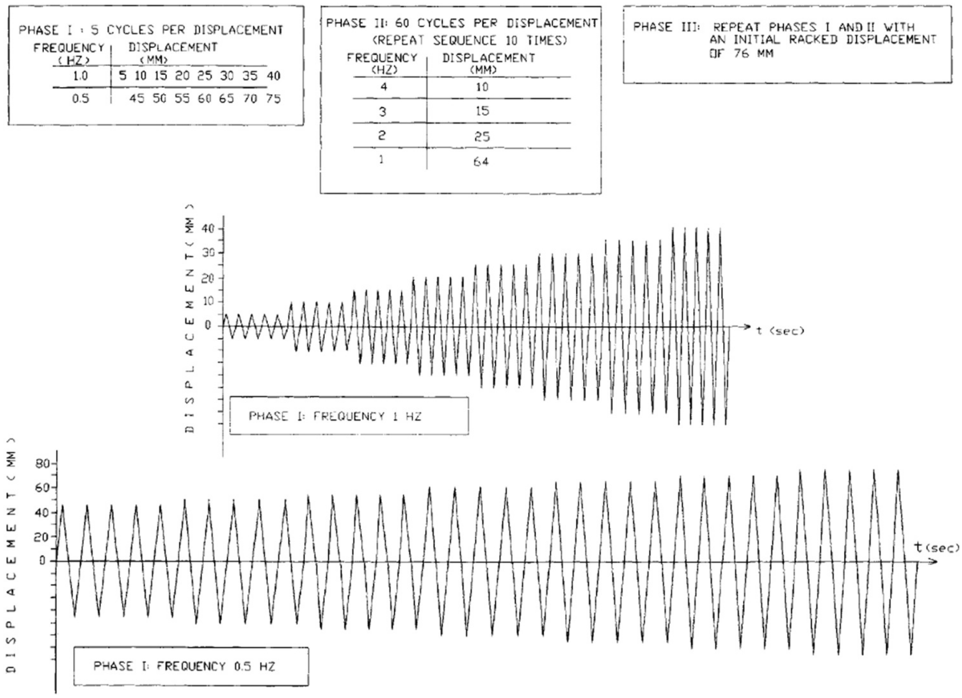

Figure 7. History of dynamic in-plane racking test displacements according to Pantelides and Behr (1994).

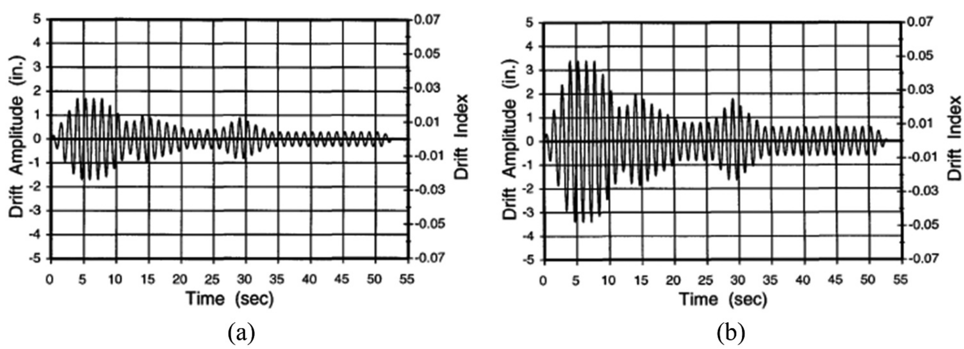

Figure 8. Drift loading histories for storefront glass serviceability (a) and ultimate (b) tests according to R. A. Behr, Belarbi, and Brown (1995).

investigate seismic serviceability limit states (Fig. 8(a)). Ultimate limit states were assessed by subjecting the storefront wall system to a loading history with doubled drift amplitudes of the serviceability test while maintaining a frequency of 0.8 hz. This amplified loading history represented a maximum credible earthquake event (Fig. 8(b)).

The test method used in the storefront study was suitable for evaluating the seismic performance of various types of architectural façade for this specific storefront building, under a specific earthquake scenario. Thus, the need for a more general test method to establish the relationship between response characteristics and performance levels of architectural façade systems gradually became evident. To move towards a more standardized test method, the so-called "crescendo test" was proposed by R. Behr and Belarbi (1996). It is a step-shaped swept sine function alternating "ramp-up" and "constant amplitude" intervals, each comprised of four sinusoidal cycles at a frequency of 0.8 hz (Fig. 9). Each

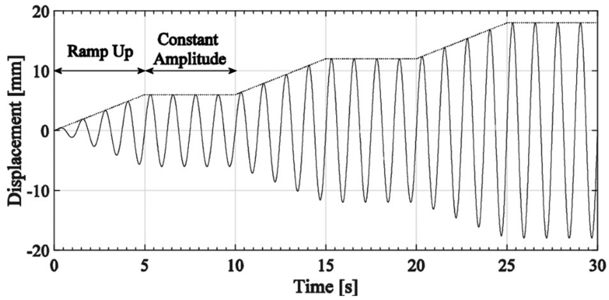

Figure 9. First part of a "crescendo test" displacement protocol according to R. Behr and Belarbi (1996).

drift amplitude step is ±6 mm. The number of cycles at each step and the test frequency were selected to be reasonable under seismic loadings. This protocol was then adopted by the American Architectural Manufacturers Association standard (2001) for seismic capacity assessment of storefront and curtain wall system.

In 2000, Brueggeman *et al.* proposed an altered application of the "crescendo" test. Hydraulic power supply and servo-actuator volumetric flow limitations required a racking frequency adjustment from 0.8 to 0.4 hz to achieve the desired dynamic drift amplitudes (Fig. 10(a)), even conducting tests where positive "half steps" and negative "half steps" are alternated (Fig. 10(b)).

Considering static or quasi-static cyclic tests, the displacement-controlled loading protocol proposed by FEMA 461 (2007) has become a widely followed protocol, suitable for various types of building envelopes. It is schematically represented in Fig. 11. The loading history consists of repeated cycles of step-wise increasing amplitudes. Two cycles at each amplitude shall be completed. The displacement amplitude for successive steps (increments) is evaluated as 1.4 times that of the step before (in Fig. 11, $a_{i+1} = 1.4{\cdot}a_i$). The protocol first requires the definition of a_0, a_{max} and n, being respectively the targeted smallest displacement amplitude of the loading history (it has to be smaller than the amplitude at which the lowest damage state is expected to occur), the targeted maximum displacement amplitude of the loading history (at which the most severe damage level is expected), and the number of steps in the loading history.

While the American standards offer more advanced and detailed testing procedures for dynamic seismic actions, the European codes provide a more flexible and generalized approach to accommodate diverse building environments. Remaining within the scope of curtain walls, for instance, EN 13830 in 2003 (CEN 2003) (first edition) provided basic performance requirements, focusing primarily on wind load resistance and thermal performance, without addressing seismic resistance. However, the subsequent revisions, particularly EN 13830:2015 (CEN 2015) and EN 13830:2022 (CEN 2022), have integrated more detailed guidelines for seismic design, in alignment with Eurocode 8 (CEN

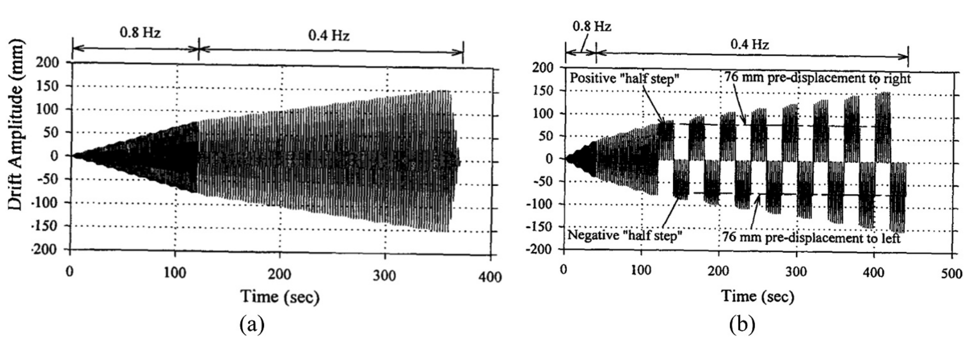

Figure 10. Drift time-histories for dynamic racking tests according to Brueggeman et al. (2000).

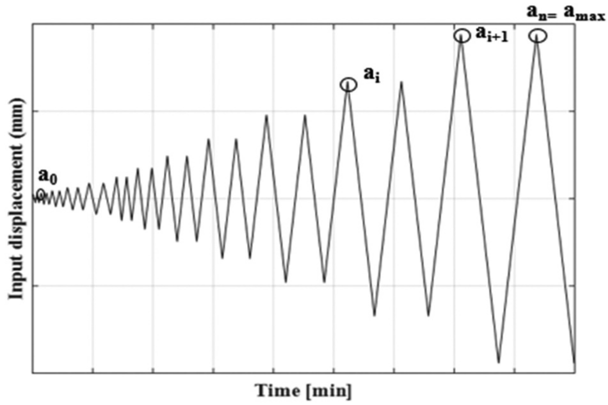

Figure 11. Displacements loading history for quasi-static cyclic tests according to FEMA 461 (2007).

2013). The 2015 version introduced the need to assess curtain wall systems under dynamic loading, incorporating both in-plane and out-of-plane seismic forces. The most recent revision, EN 13830:2022, further refined these seismic design requirements, however without providing detailed guidance on experimental procedures and methods for measuring demand and capacity. In this sense, it aligns with Eurocode 8's broader, more generalizable framework for seismic safety across building components. On the contrary, as said, the American codes generally provide more granular, component-specific testing protocols.

Based on the existing literature and codes summarized above, in Section 3, alternative protocols will be presented, emphasizing the strengths of the different above proposals while attempting to overcome some of their inherent limitations. Some of the proposed advancements (e.g. cyclic and dynamic testing at higher frequencies, aiming to replicate those typically induced by earthquakes) are now feasible due to the availability of highly advanced and high-performance machinery. Specifically, a modified crescendo test will be proposed as a quasi-static test, particularly suitable for evaluating the in-plane response of non-structural components, and a method based on the selection and reproduction of spectrum-compatible accelerograms will be proposed as dynamic test for out-of-plane tests.

3. Test Equipment and Loading Protocols for Seismic Capacity Assessment of Building Envelopes

This section describes the main results of a decade of research efforts aimed at overcoming the limitations summarised before in terms of both testing equipment and corresponding protocols. These results are shown in terms of both main features of the testing facility and input loading protocols that should be adopted for the evaluation of the seismic capacity of building envelope elements, like external wall claddings mechanically fixed and connections for precast concrete façade panels.

3.1. Test Equipment

A suitable testing equipment should allow the installation of full-scale plane envelope systems, the reproduction of the real installation conditions and to apply both quasi-static and dynamic actions to completely assess the seismic behavior of several typologies of building envelopes elements.

One of the most advanced machines currently dedicated to applications of this kind is located at the Institute for Construction Technologies (ITC) of the Italian National Research Council (CNR), in the laboratory of San Giuliano Milanese (Milan, Italy). This equipment allows the installation of full-scale plane systems up to 5,600 mm (width) and 8,000 mm (height). The test

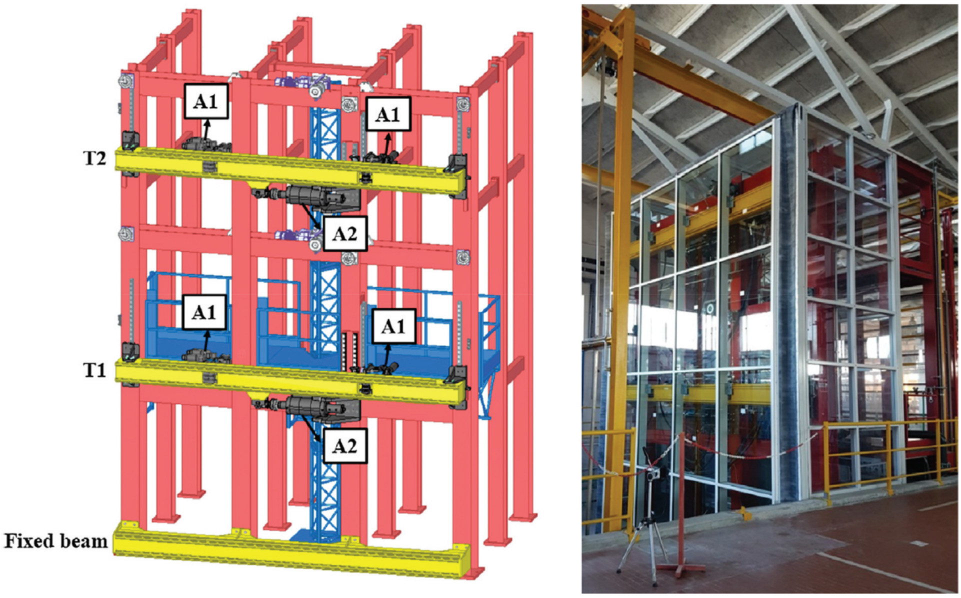

Figure 12. Schematic view of the ITC-CNR test facility (left) and picture (right).

specimen can be mounted on a steel framed structure at three levels, with a fixed beam at the base (Fig. 12) and two moveable beams at the second and third levels (T1 and T2 in Fig. 12). All beams are equipped with anchoring channels, in order to enable the installation of various types of façade systems and partition walls. The moveable beams are connected to a system of dynamically controlled hydraulic actuators. A mechanical lifting system of the beams allows to obtain different inter-story heights. The displacements in the plane of the specimen are produced by a double rod hydraulic actuator, indicated as A2 in Fig. 12, positioned on each mobile beam, with a load capacity of 200 kN and a maximum displacement of ±85 mm. It is possible to apply displacements in dynamic condition with high frequencies, up to 30 hz. The two hydraulic actuators are able to work in counter-phase to obtain inter-story displacement (between the second and third levels) up to 170 mm. Instead, the displacement in the out-of-plane direction is produced by a double rod hydraulic actuator (type A1 in Fig. 12). They are two for each beam with a load capacity of 100 kN and a maximum displacement of ±85 mm. It is possible to apply displacements in dynamic condition with relatively high frequencies. The actuators are interfaced with a control system that allows to apply the desired displacement histories and amplitudes, frequencies and number of cycles.

3.2. Loading Protocols

A suitable loading protocols for the seismic capacity assessment of building envelopes should consider both static or quasi-static and dynamic tests. The application of cyclic loads in quasi-static conditions allows for a more accurate identification of the damages occurred in the specimen during a seismic test, thanks to the limited load application speed. On the other hand, it is also important to study the effects of loads applied in dynamic conditions on the tested components, in order to better simulate the effects of real earthquakes. For the above-mentioned reasons, a comprehensive experimental campaign aimed at evaluating the seismic capacity of envelope elements should provide for both quasi-static and dynamic tests.

Even after a selection of a loading protocol, however, the choice between carrying out tests in the in-plane and in the out-of-plane directions of the component simultaneously or in uncoupled way is not straightforward. It clearly depends on the features of the selected building envelope components in terms of masses, stiffness and connection typologies with the main structures. The experience with seismic tests on several kinds of envelope products has led to the identification of different loading procedures, selected case by case. Details of testing activities are shown in Section 4 for external wall claddings mechanically fixed and in Section 5 for heavy precast panel façade and their connection devices to the main structure.

The following paragraphs detail the quasi-static (Section 3.2.1) and dynamic (Section 3.2.2) test loading protocols that should be adopted for building envelope elements.

3.2.1. Quasi-Static Tests

As said in Section 2.2, a consolidate approach to perform quasi-static tests on building envelope components is the so called "crescendo test" by AAMA 501.6 (2001), first proposed for curtain wall and storefront systems. It consists of a concatenated series of a group of "ramp up" cycles and a group of "constant amplitude" cycles. Each group is made of four sinusoidal cycles. Each "ramp up" group leads to a displacement demand increase equal to 6 mm. The dynamic frequencies are equal to 0.8 hz at lower amplitudes (i.e. up to ±75 mm) and equal to 0.4 hz at higher amplitudes (i.e. greater than ±75 mm). Differently from the original version from AAMA, a modified crescendo test is proposed herein. The rationale for proposing this upgrade to the conventional AAMA approach is to impose more stringent demands on the tested component, particularly in terms of velocity: instead of the above 0.8 hz and 0.4 hz values of frequency, this version suggests using 2 hz and 1 hz, respectively (Fig. 13) compatible with the capabilities of the testing machine.

As for the "original" method, the test shall be run continuously until the first of the following condition exists:

- fallout of any component of the assembled envelope kit,
- the maximum applied displacement is equal to ±150 mm.

A video recording of the test, synchronized with the clock of the testing apparatus, is highly recommended for off-line processing and temporal positioning of damage evolution.

3.2.2. Dynamic Tests

Especially for acceleration-sensitive components, it can be crucial to conduct tests with higher dynamic characterization in respect to those quasi-static ones described in the previous section. The approach herein suggested for dynamic tests is based on the use of artificial accelerograms, allowing more selective signals with higher and uniform energy content over a wider frequency

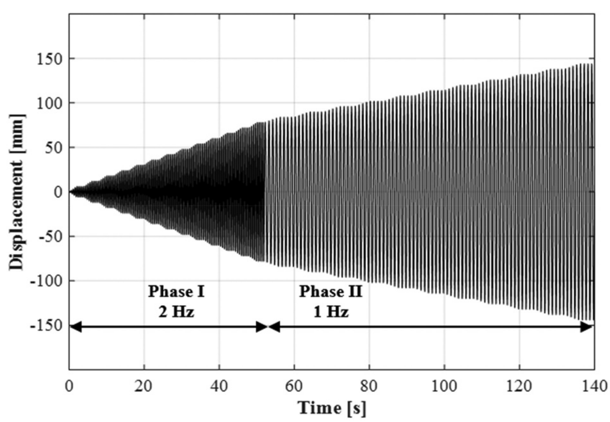

Figure 13. Modified crescendo test.

band, and the testing procedure is implemented according to the shake table protocol defined by Zito, D'Angela, et al. (2022). It consists in the application of a series of artificial acceleration time-histories having increasing intensity. The reliability of the abovementioned protocol was analytically assessed by D'Angela et al. (2024) considering inelastic single-degree-of-freedom systems, and it resulted overall satisfactory, especially considering reference alternative protocol such as ICC-ES (2020). More in detail, the loading procedure can be summarized in the following steps:

(1) At first, the input acceleration time-history shall be obtained. In order to define the input acceleration time history, it is necessary to define a Reference Response Spectrum (herein after RRS). The RRS (Fig. 14) can be assumed equal to a special version (Zito, D'Angela, et al. 2022) of the spectral acceleration formulas reported in clause 4.3.5 of EN 1998–1 (CEN 2013). The latter is evaluated in the time domain, according to Eq. 1 , or in the frequency domain, according to Eq. 2 (Fig. 14).

$$\begin{cases} \frac{S_a}{(\alpha)} = \left[\frac{10}{1+4\left(1-\frac{T_a}{T_0}\right)^2}\right] & T_a \geq T_0 \\ \frac{S_a}{(\alpha)} = 10 & T_0 \leq T_a < T_1 \\ \frac{S_a}{(\alpha)} = 8 + \frac{2}{(T_1 - T_2)}(T_a - T_2) & T_a \geq T_1 \end{cases} \tag{1}$$

$$\begin{cases} \frac{S_a}{(\alpha \cdot S)} = 8 + \frac{2}{(f_1 - f_0)}(f_a - f_0) & f_a < f_1 \\ \frac{S_a}{(\alpha \cdot S)} = 10 & f_1 \leq f_a < f_2 \\ \frac{S_a}{(\alpha \cdot S)} = \left[\frac{10}{1+4\left(1-\frac{f_2}{f_a}\right)^2}\right] & f_a \geq f_2 \end{cases} \tag{2}$$

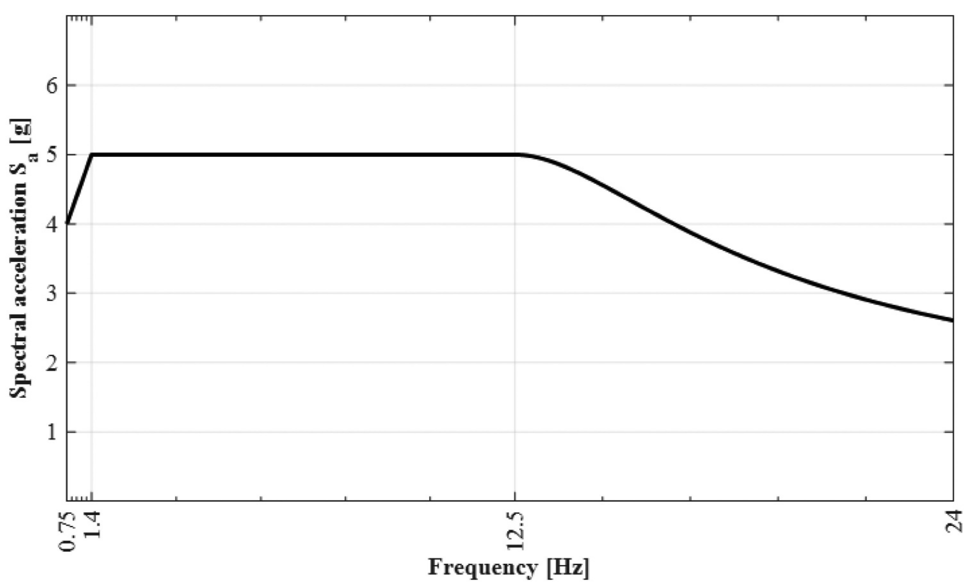

Figure 14. Reference response spectrum (RRS) in the frequency domain, 5% damped.

where:

- S_a is the spectral acceleration used to calculate the horizontal equivalent static force to be applied to the non-structural elements;
- α is the ratio between the reference peak ground acceleration on stiff soil for the considered limit state and the acceleration of gravity;
- S is the soil amplification factor;
- T_a is the fundamental vibration period of the non-structural element;
- T_0 is the starting period of the RRS and is equal to 0.08 s;
- T_1 is the period corresponding to the beginning of the constant acceleration branch of RRS and is set to 0.714 s;
- T_2 is the period corresponding to the last descending branch of RRS and is equal to 1.33 s;
- f_2, f_1 and f_0 are the frequencies corresponding to the periods T_0, T_1 and T_2 assumed equal to 0.75·Hz, 1.4 hz and 12.5 hz, respectively.

Starting from this RRS, an acceleration time-history shall be chosen in a manner that the relative spectrum (called Test Response Spectrum – TRS) shall be compatible with the RRS, defined assuming α·S = 0.50 g, over the frequency range 1.4–24 hz. The starting acceleration time-history shall be a nonstationary broadband random excitation having an energy content ranging from 1 to 32 hz and a bandwidth resolution equal to one sixth-octave. The total duration of the input motion shall be 30 seconds, which includes 5 seconds for the acceleration ramp-up, 20 seconds of strong motion time duration and 5 seconds for the decay time. The amplitude of the narrowband signal shall be adjusted until the TRS envelops the RRS. It is recommended that the TRS shall be between 130% and 90% of RRS. The obtained acceleration time-history shall be also compatible with the test equipment limitations. For this purpose, a "filter tool" can be used to generate a signal compatible with the maximum accelerations (or displacements) applicable by the test equipment. In particular, the signal can be filtered through high-pass filters considering a maximum frequency threshold equal to 0.75 f_a, bounded in any case at 3.5 hz.

The maximum acceleration value of the input acceleration time history is defined as a_{max} (Fig. 15).

(2) Several acceleration time-histories shall be obtained by linearly scaling down the input acceleration time-history defined above. It is recommended, when possible, to proceed in small incremental steps, for example starting from a 5% scaling value and reaching 100% with progressive 5% increments. Each acceleration time-history formally corresponds to a sub-step of the test. If it is expected that accelerations lower than 5%·a_{max} can affect the integrity of the component, lower initial accelerations can be considered as well. The test shall continue up to either the failure of the specimen or the attainments of the test facility limits.

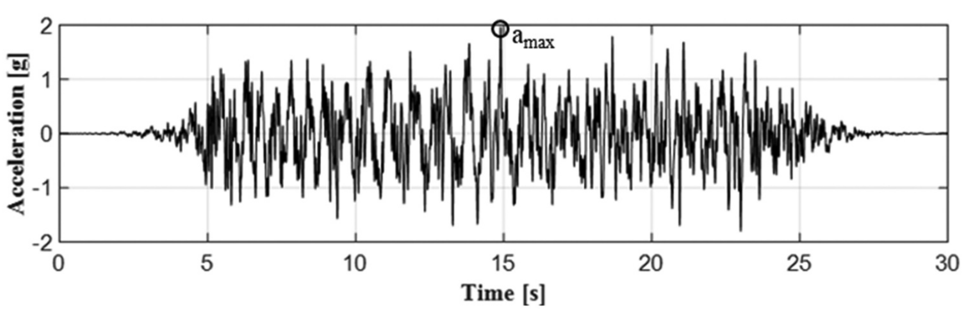

Figure 15. Example of input acceleration time-history.

4. Assessment Procedures for Seismic Capacity of External Wall Claddings

Based on what is described above about the testing facility and the loading protocols, this section describes an assessment procedure aimed at the evaluation of the seismic capacity of external wall cladding.

Generally, the seismic capacity of envelope components can be schematically described by means of two engineering demand parameters (EDP):

(i) the out-of-plane acceleration recorded in the center of masses of the kit, since they can be considered acceleration-sensitive components in the out-of-plane direction;
(ii) the in-plane inter-story displacements, since these components can be considered drift-sensitive in the in-plane direction.

In order to define the seismic capacity of the external wall cladding in terms of out-of-plane accelerations, a_{OOP}, and the in-plane displacements, $\Delta_{dmax,IP}$, it is necessary to assume appropriate loading protocols for their experimental assessment. This aspect was discussed in the previous sections, however it will be revisited and detailed later on for the specific case of interest.

It is then important to identify the appropriate damage states (DSs) for the specific component under examination, so that, through testing, a specific value (capacity) can be assigned to each of the two EDPs for each said damage state. Three DSs can be defined for nonstructural envelope components:

(1) DS1 – “Minor damage” state: minor damage state achievement implies the need to slightly repair the envelope component to restore its original condition.
(2) DS2 – “Moderate damage” state: moderate damage state achievement implies that the envelope component is damaged so that it shall be partially replaced.
(3) DS3 – “Major damage” state: major damage state implies that the damage level is such that either the envelope component needs to be totally replaced or the life safety is not ensured.

Returning to the experimental protocols, according to the experience gained by the authors, the two EDPs should be assessed in an uncoupled manner:

- out-of-plane acceleration capacity at the three DSs, say $a_{DS1,OOP}$, $a_{DS2,OOP}$, $a_{DS3,OOP}$, shall be assessed by means of the dynamic tests with artificial accelerograms described in Section 3.2.2;
- in-plane capacity displacements for each of the three DSs, say $\Delta d_{max,DS1,IP}$, $\Delta d_{max,DS2,IP}$, $\Delta d_{max,DS3,IP}$, shall be assessed by means of modified crescendo test described in Section 3.2.2.

The proposed methodology has been validated for ventilated facades, as reported in the European harmonized technical specification EAD 090062-01-0404 (EOTA 2021) and schematically summarized in Section 4.2, but further experimental tests, designed by the Authors and currently in progress, are demonstrating that such methodology can be properly implemented also for curtain walls and precast facades systems.

4.1. Test Specimen and Test Setup

The specimen to test shall fully reflect the assembled cladding kit, including all necessary fittings, fixings and joints. It shall include all integral components which may have a detrimental effect on the seismic performance of the kit. The dimensions of the test specimen depend on the size of the cladding element and on the specified cladding fixings. In general, when possible, an odd number of cladding elements shall be considered both in horizontal and vertical direction.

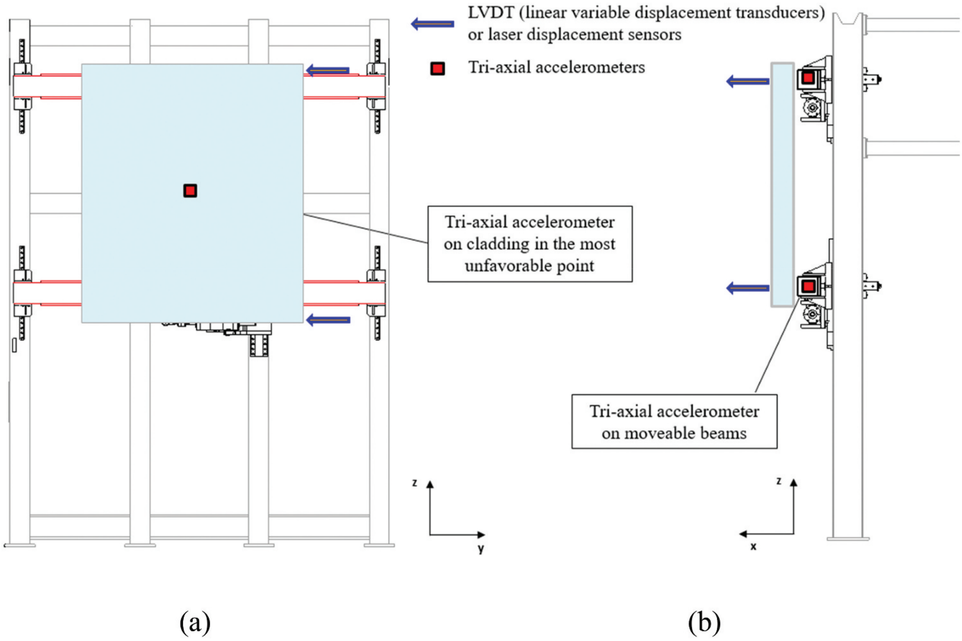

Figure 16. Example of monitoring system: (a) frontal and (b) lateral view.

Tests shall be carried out by using a test equipment capable to replicate both dynamic and quasi static loading protocols with at least two degrees of freedom in the plane and out of the plane of the component, like that shown in the previous section (Fig. 12).

The monitoring system shall be constituted, as minimum, by:

- displacement sensors (e.g. laser displacement transducers), located at the bottom and at the top of the specimen to monitor the in-plane and out-of-plane displacements of the cladding elements (see Fig. 16).
- Tri-axial accelerometers located at least in the most unfavourable point of the cladding element closest to the geometric centre of the assembled kit (see Fig. 16(a)), and on the movable beams (see Fig. 16(b)). The analysis of 3D accelerations may help to better interpret the test results, also helping to reveal any anomalies (e.g. unexpected vertical accelerations may help understand that the specimen is not properly fixed).

4.2. Preliminary Assessment of a Case Study Wall Cladding

In this section, with reference to a specific case study, the previously described seismic performance evaluation approach is partially revisited, after a deep analysis of some of the most significant steps of the testing protocol. The objective is twofold: to identify any peculiarities or critical issues, and to detect those aspects of the experimentation that are necessarily dependent on the specific object being tested.

The test specimen is a ventilated façade system. It has dimensions of 2.405 m (width) x 4.128 m (height), as shown in Fig. 17(a), and it is constituted by an assembly of 10 mm thick porcelain stoneware panels, connected by means of fixing hooks (“S10 hook” in Fig. 17(b)) to a subframe of vertical uprights consisting of 2 mm thick T-profiles (“trust80” in Fig. 17(b)) in raw aluminum alloy (dimensions 110 mm × 80 mm), positioned at a distance of 1.200 m. L-shaped support

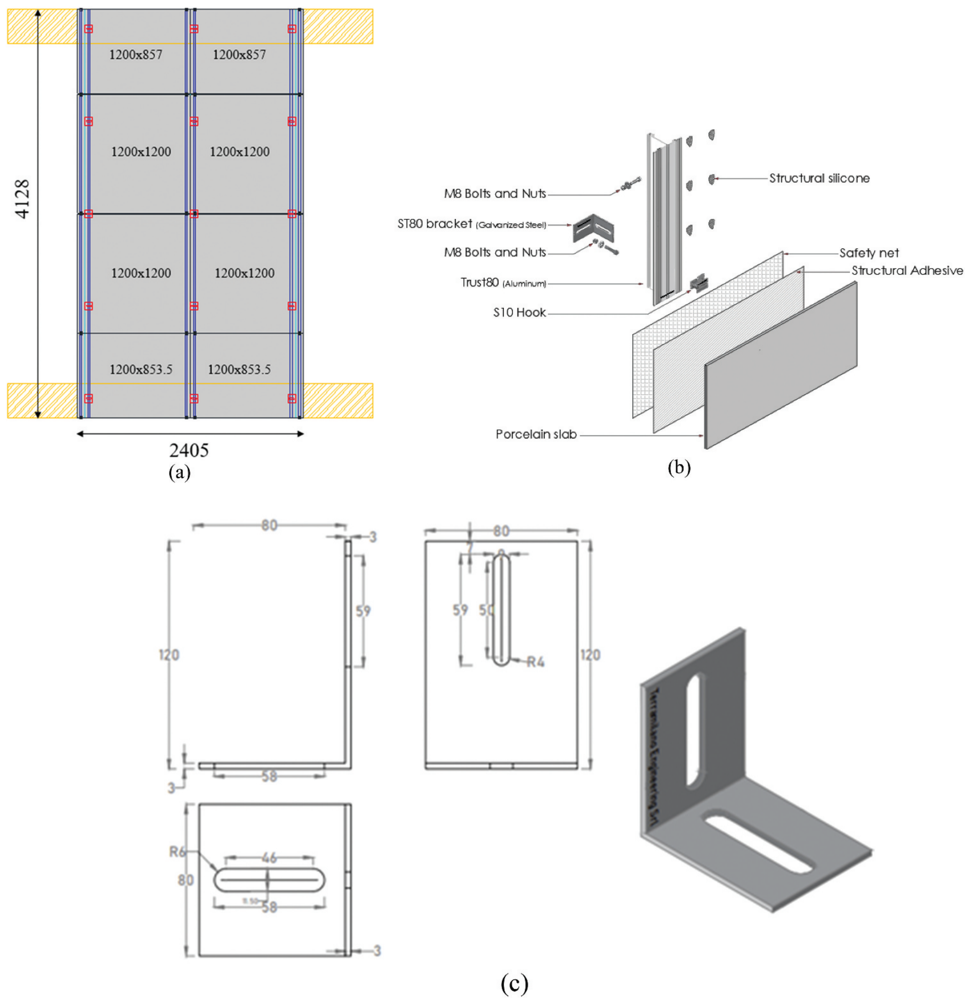

Figure 17. (a) Dimensions of the tested sample, with (b) construction details and (c) particular of L-shaped support brackets (in mm).

brackets (Fig. 17(c)) in galvanized steel S235 allow the connection of the subframe to the main structure.

For the execution of the tests and in order to reproduce the real installation conditions, the subframe vertical studs of the cladding kit were connected to a substructure consisting of three steel tubular profiles S235JR (refer to Fig. 18(a)) 3.900 m long and with a section 60 × 60 x 4 mm. The latter have been connected to the beams of the equipment used for the seismic tests to simulate an external wall which the analyzed cladding kit is attached to. The test setup implemented follows the movements of the primary structure, which are simulated using the seismic equipment described in Section 3. These movements are directly transferred to the system under study. Fig. 18 shows some mounting phases of the ventilated façade system and a complete view of the tested specimen (Fig. 18(d)).

According to the general procedure explained in Section 4, the specimen has been subjected to:

- out-of-plane dynamic tests with artificial accelerograms to assess the acceleration capacity at the different DSs ($a_{DS1,OOP}$, $a_{DS2,OOP}$, $a_{DS3,OOP}$);
- the in-plane modified crescendo test to assess the displacement capacity at the various DSs ($\Delta d_{max,DS1,IP}$, $\Delta d_{max,DS2,IP}$, $\Delta d_{max,DS3,IP}$).

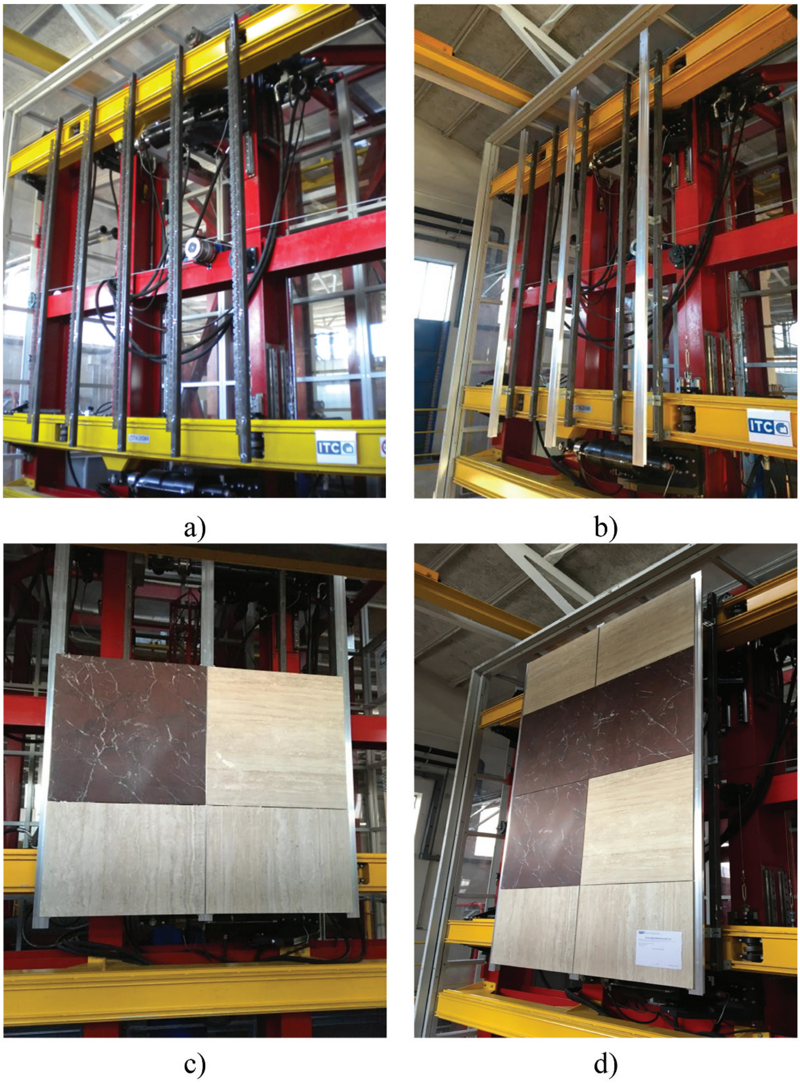

Figure 18. Construction phases of the test specimen.

A damage scheme, still framed within the general framework proposed in the previous sections, must be defined to handle in appropriate detail the potential damage manifestations of the specific component under examination. The damage scheme adopted is summarized in Table 1. It allows the identification of the damages than can occur in each component of the kit for each of the three conventional damage levels. The results of the tests performed are reported in the following sections.

4.2.1. Dynamic Tests: Results and Discussion

Dynamic tests have been performed using artificial input acceleration time-histories with increasing intensity as introduced in Section 3.2.2. A starting acceleration time-history is selected and iteratively modified, using the RSP Match software (Hancock et al. 2006), in such way that it its own Test Response Spectrum-TRS was spectrum compatible with the RRS. The latter has been defined selecting the parameters detailed in Eq. 1 and Eq. 2 of Section 3.2.2 and assuming $\alpha \cdot S = 0.50$ g in order to consider the spectrum at ultimate limit state and in high seismic zone, over the frequency range 1.4–24 hz. The acceleration spectra after the

Table 1. Damage scheme for external wall claddings mechanically fixed.

Component of the assembled cladding kit	Damage type		
	DS1 - Minor damage state	DS2 – Moderate damage state	DS3 – Major damage state
Cladding elements	Slight in-plane or out-of-plane cladding element rotation.	Significant out-of-plane cladding elements rotations. Minor cracks in cladding elements providing fall out of pieces with mass equal or less than 0.2 kg.	Cladding elements overturning providing fall out of pieces with mass more than 0.2 kg.
Cladding fixings	Failure of at least 10% of the total amount of cladding fixings.	Failure of at least 30% of the total amount of cladding fixings	Failure of at least 50% of the total amount of cladding fixings
Subframe components (vertical and/or horizontal profiles, brackets, screws, metal anchors)	Minor plastic deformations of profiles. Failure of at least 10% of total brackets, screws, and metal anchors.	Moderate plastic deformations of profiles. Failure of at least 30% of total brackets, screws, and metal anchors.	Severe plastic deformations of profiles. Failure of at least 50% of total brackets, screws, and metal anchors.
Thermal insulation products	No damage.	Collapse of thermal insulation product with a mass equal or less than 0.2 kg.	Collapse of thermal insulation product with a mass more than 0.2 kg.
Ancillary components (breather membrane, cavity barrier, joint-covers, gaskets, trims)	No damage.	Collapse of an ancillary component with a mass equal or less than 0.2 kg.	Collapse of an ancillary component with a mass more than 0.2 kg.

matching procedure (TRS) is shown in Fig. 19 while the spectrum compatible input profiles in terms of acceleration (a_{max} = 1.97 g), velocity and displacement (d_{max} = 139 mm) are reported in Fig. 20.

Incremental intensity accelerograms were generated by scaling down the reference accelerogram described above, in accordance with the procedure in Section 3 and simultaneously applying both at the bottom and at the top beam of the specimen, in the out-of-plane direction, in a displacement-

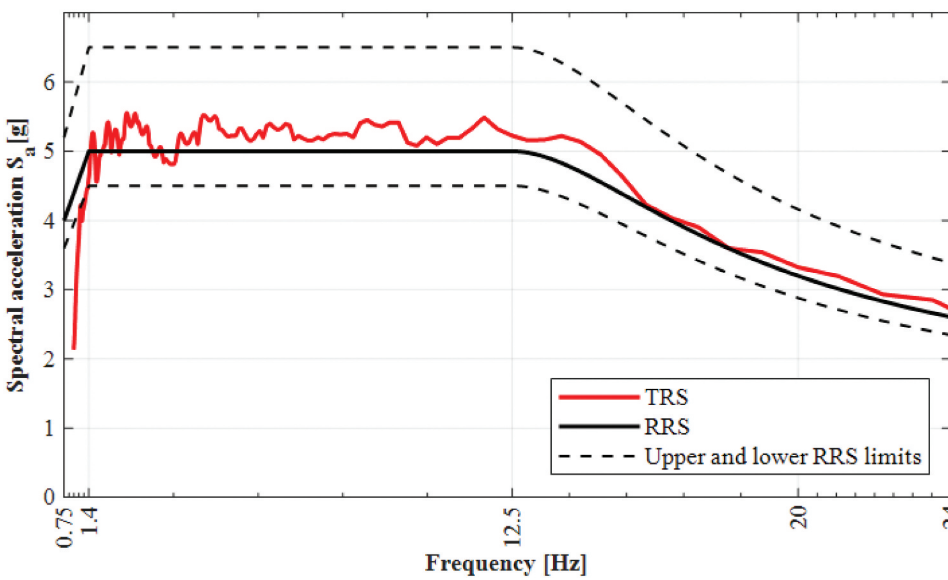

Figure 19. Acceleration spectra for spectrum-compatibility check.

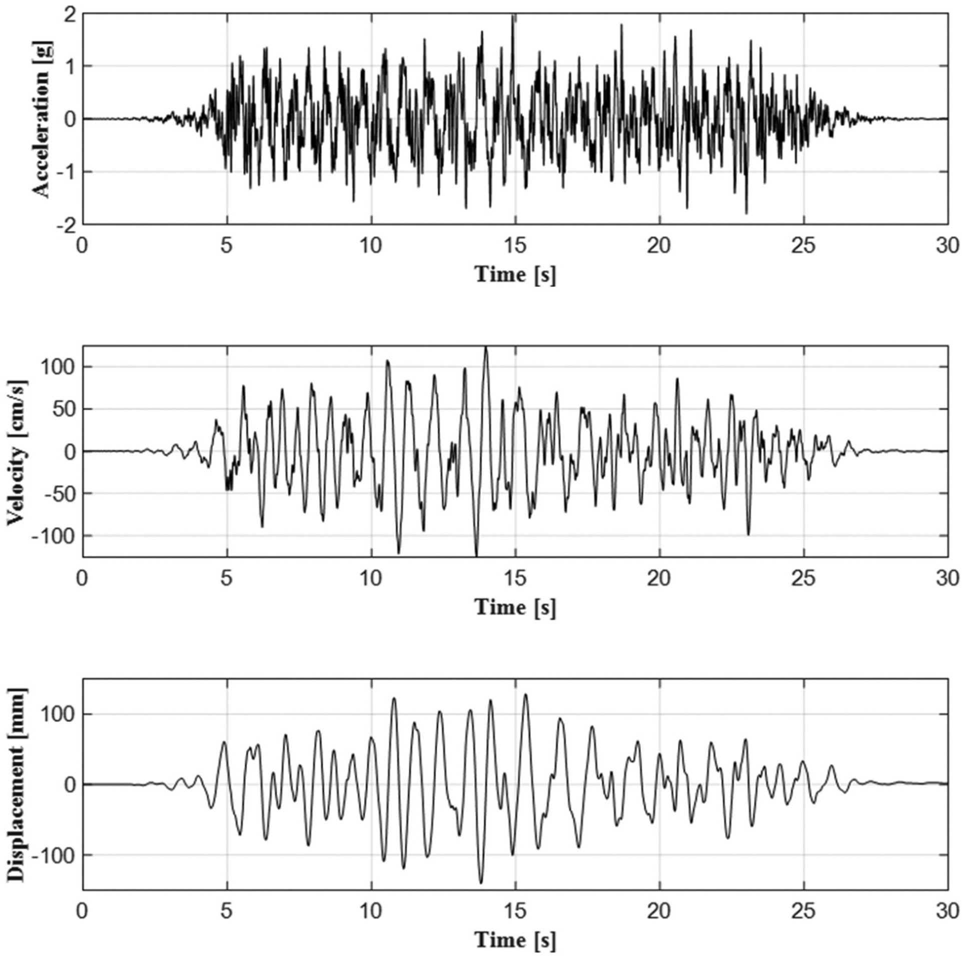

Figure 20. Spectrum compatible input profiles in terms of acceleration, velocity and displacement.

control framework. In Fig. 21 the displacement profiles applied to the T1 beam for tests corresponding to 10%, 20%, 30%, 40%, 50% and 60% of d_{max} are shown.

In terms of accelerations, recorded in the center of the porcelain stoneware panel closest to the geometric center of gravity of the specimen (Fig. 22), it can be seen (Fig. 23) a quite linear increasing trend up to test with scale factor of 0.5 where the peak acceleration to the component resulted to be about 2.5 g. A very sudden change in trend is observed for the scale factor of 0.6, when the recorded peak acceleration was 6.25 g. After this test, no visible damage was evident. However, the drastic change in the dynamic behavior of the panel must necessarily be linked to some form of damage, even if minor, likely in the connections. In this application, the level of recorded acceleration (2.5 g) at the sub-step with 0.5 scale factor, is labeled as out-of-plane acceleration capacity corresponding to the achievement of DS1 (Table 2). Then, since no further damages are recorded until the end of the test, it can be assumed that the out-of-plane acceleration capacities corresponding to the achievement of DS2 and DS3 is greater than 6.25 g.

4.2.2. Modified Crescendo Test: Results and Discussion

After the dynamic test, a new specimen has been subjected to the in-plane displacement profile provided by the modified crescendo test (Section 3.2.2). Damage of each component of the assembled cladding kit has been recorded during the tests by filling out the damage scheme. The measured relative displacement between the base and the top of the specimen corresponding to the achievement

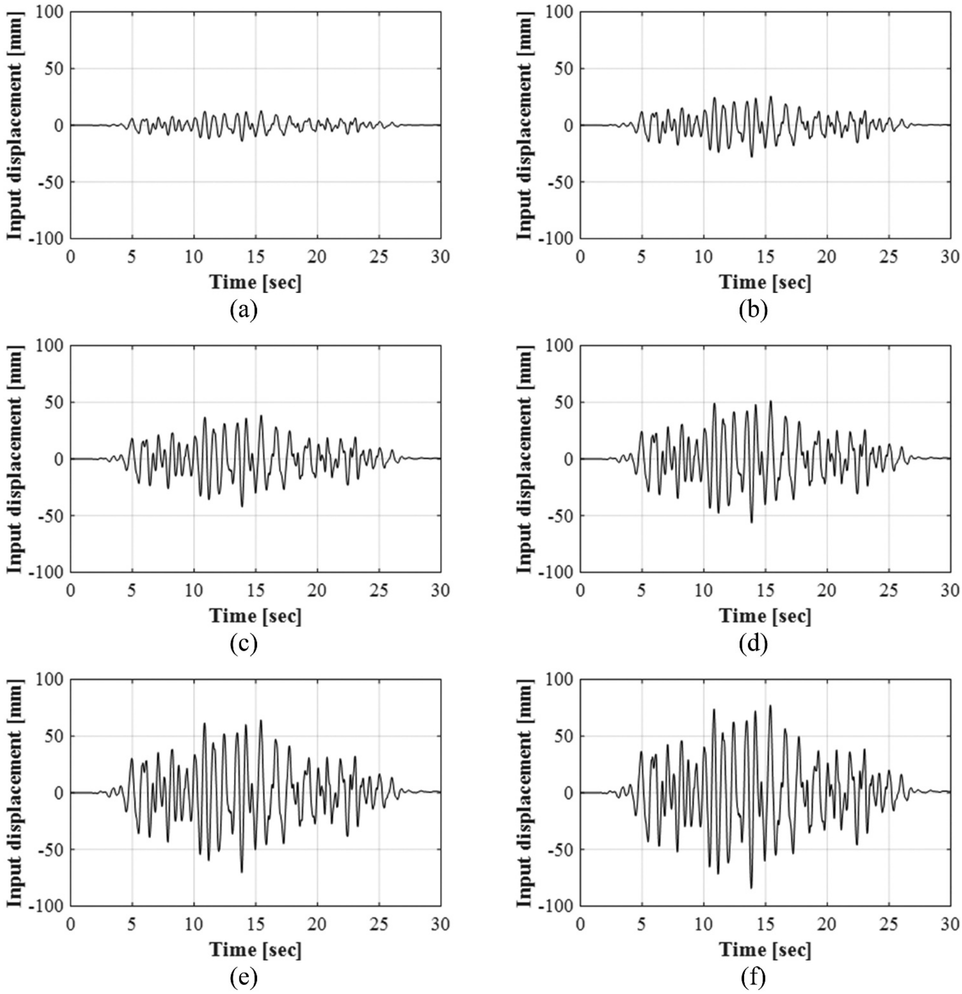

Figure 21. Displacement time-histories applied to the specimen at (a) 10%, (b) 20%, (c) 30%, (d) 40%, (e) 50% and (f) 60% of the maximum intensity.

of each damage state represents the in-plane direction displacements $\Delta d_{max,DSi,IP}$ of the specimen, where i = 1, 2 or 3 refers to the defined damage states.

Subjected to the complete (modified) crescendo test the sample showed the following damages:

- the first damage consisted in the fall of a small portion in the corner of the porcelain tile where it is connected with the clip to the stud (position 1 in Fig. 24(a)). The damage occurred for an applied inter-story displacement of 35 mm, corresponding to an inter-story drift of 1.1%;
- by further increasing the displacements up to 40 mm (drift = 1.25%) a detachment of the same portion of an underlying tile is observed (position 2 in Fig. 24(a));
- at 47 mm (drift = 1.47%) applied displacement, a further detachment of a portion of the tile, again at the connection point with the stud (position 3 in Fig. 24(a)), occurs;
- starting from the applied displacements of about 53 mm (drift = 1.65%) a strong rotation of the external right stud was observed. It was due to the bolt leaving the guide (Fig. 24(b)). Inspecting the back of the sample at the end of the test, it was observed that the left and central side studs did not show rotations, but the damage was concentrated in the bottom brackets which reached yielding.

Figure 22. Position of the accelerometer on the tested specimen.

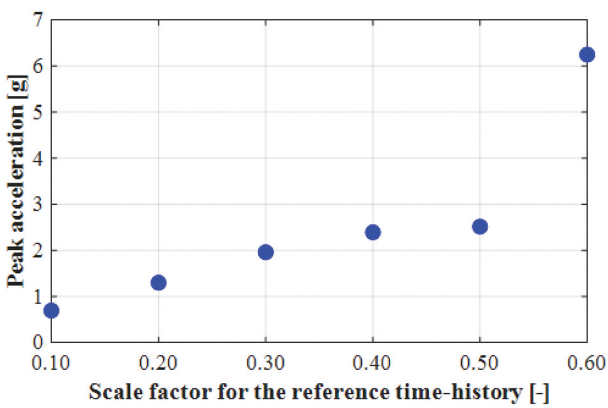

Figure 23. Recorded peak accelerations in the panel for each dynamic test.

The test was conducted for displacements up to 150 mm, in accordance with the protocol, with no significant changes in the damage state.

Comparing the above-described recorded damages with the damage scheme defined in Table 2, it is possible to define the seismic capacity of the specimen in terms of in-plane displacements, according to Table 3. In particular:

Table 2. Value of out-of-plane acceleration capacity for each damage state.

Damage type		
DS1 (minor damage)	DS2 (moderate damage)	DS3 (major damage)
Peak acceleration a_{OOP} [g]		
>2.5	>6.25	>6.25

Figure 24. Damages occurred during the in-plane crescendo test: (a) detachment of portion of porcelain tiles; (b) brackets bolt leaving the guide and (c) yielding of the bottom brackets.

Table 3. Value of in-plane displacement corresponding to the achievement of DSi.

Damage type		
DS1 (minor damage)	DS2 (moderate damage)	DS3 (major damage)
	Interstory displacement $\Delta d_{max,DS}$ [mm]	
–	35 (drift ratio 1.1%)	53 (drift ratio 1.65%)

the first recorded damage, i.e. the failure of a small portion of the cladding elements, can be assumed corresponding to the achievement of DS2. It happens for a 35 mm inter-story displacement;

the rotation of the stud, due to the failure of the brackets, occurred for 53 mm inter-story displacement, can be assumed corresponding to the achievement of DS3.

5. Assessment Methodology for Seismic Capacity of Connections for Precast Concrete façades

This section describes a new methodology for the seismic assessment of the connection devices for cladding panels in precast buildings, referring to the testing facility and the loading protocols defined in the previous sections.

The façade system for typical European one-story precast buildings, especially used for industrial and commercial purposes, is made of horizontal or vertical precast concrete panels attached to the main building by means of steel connections. This paper focuses on vertical panels and on the seismic behaviour of an innovative connection system used to link the panels to the main structure. Due to the huge mass of the above-mentioned precast panels, the connection systems should be conceived to reduce dynamic interaction with the main structure. For this reason, the most widely adopted connection scheme allows panel-to-structure displacements in the plane of the non-structural component while restraining the out-of-plane overturning.

The innovative connection system considered in the following is able to connect cladding elements and structure allowing free movements in different directions (horizontal and vertical) in order to absorb relative displacements and to transfer the resulting forces during an earthquake.

Therefore, such non-structural components can be considered drift-sensitive for in-plane loads, force-sensitive in the out-of-plane direction. Consequently, the relevant EDPs for this kind of cladding system are the out-of-plane force and the in-plane panel-to-structure displacement.

In particular, for such component a specialized methodology described in the following sections is proposed, based on the general approach discussed in Section 3. More in detail, the assessment of the seismic behaviour of panel-to-structure connections needs accurate consideration of simultaneous in-plane and out-of-plane actions. This is significant for both seismic demand and capacity of the component. Therefore, for such components it turned out from the testing activity that an appropriate approach should consider bidirectional dynamic tests (demand) as well as to identify the seismic capacity by means of an interaction chart based on the combined action of the two selected EDPs.

Representative damage states for such kind of panel-to-structure connections have been selected referring to the device capability to provide an effective constrain for the cladding system towards seismic actions, as described in the following:

(1) DS1 – Operational level: no damage recorded and the device preserves its full functionality towards seismic actions;
(2) DS2 – Life safety level: detachment of concrete portions surrounding the anchor channel which can be dangerous for occupants or fleeing persons;

(3) DS3 – Collapse prevention level: yielding of bolts or steel plates of the connection system, connection system failure so that the device is not able to guarantee an effective constrain with the consequent precast panel detachment.

5.1. Test Specimen and Test Setup

The panels studied in this article are those commonly used in single-story precast RC structures. The setup involves installing a full-height vertical panel, anchored at the base with a bolted connection and at the top with the connectors under investigation. The specimen is instrumented with displacement and acceleration transducers to continuously obtain the two reference EDPs. Further details about geometry of the panel, the sensors and the definition of the acceleration-displacement interaction chart are provided in the subsequent section, which pertains directly to a concrete application in a case study.

5.2. Preliminary Assessment of a Case Study Connection System for Precast Concrete Façades

In this section, with reference to a specific case study, the previously described seismic performance evaluation approach is partially revisited, again to analyse some of the most significant steps of the testing protocol. The primary objective in this case is to show how the data recorded in the experimental tests of precast concrete façades can be processed to define a special kind of capacity domain for the panel-to-structure connections. The suggested methodology introduces a new design criterium based on the definition of "capacity boundaries." This methodology can be applied to a wide variety of devices, and it is detailed in the following, for demonstration purposes only, considering the innovative connection system described above. With reference to the selected connection device, the capacity boundaries have been defined in the Cartesian plane out-of-plane accelerations vs in-plane mutual displacements but they can consider different EDPs or they can be extended to multi-dimensional domains for different connection devices.

The scheme of the studied panel-to-structure connection system is reported in Fig. 25. This system generally allows the connection of both vertical and horizontal precast concrete cladding panels to beams and columns, respectively: in this paper the application for vertical panels connected to horizontal beams is considered. The connection device is constituted of anchor channels embedded in the precast elements (panel and beam/column); the ribbed steel plate and the bolt allow the regulation of the system during the assembly phase. The nuts, pre-inserted in the anchor channels, can slide and allow the relative displacements between the panel and the main structure, both in horizontal and vertical direction.

The full scale test setup consists of a 2.5 m wide, 7.0 m high and 0.3 m thick vertical precast concrete cladding panel with a core of insulating material and a total mass of 6.3 Mg, connected to the seismic machine through two connection systems (Fig. 26(a,b)). For each of them, an anchor channel is embedded in the precast panel, while a second one, usually embedded in a perimetral precast concrete beam, was inserted in a steel apparatus designed *ad hoc* to reproduce the real concrete confinement of the connection device in the beam. The steel apparatus is fixed to the upper movable beam of the testing machine (T2 in Fig. 12), properly positioned to connect to the panel at 6.5 m (Fig. 3). The panel is fixed to the basement by means of bolted steel connections.

The testing monitoring system is schematically represented in Fig. 27. It consists of: (a) two linear variable displacement transducers (LVDT), to measure panel to-beam horizontal displacements in the out-of-plane (LVDT 1) and in-plane (LVDT 2) direction; (b) two monoaxial accelerometers to measure the panel acceleration in the out-of-plane (ACC1) and in-plane (ACC2) directions.

5.2.1. In-Plane and Out-Plane-Dynamic Tests

The dynamic tests have been performed according to the test procedure reported in Section 3.2.2 using the same artificial accelerograms introduced in Section 4.2.1. In this case, the increasing levels of acceleration time-histories are those reported in Table 4.

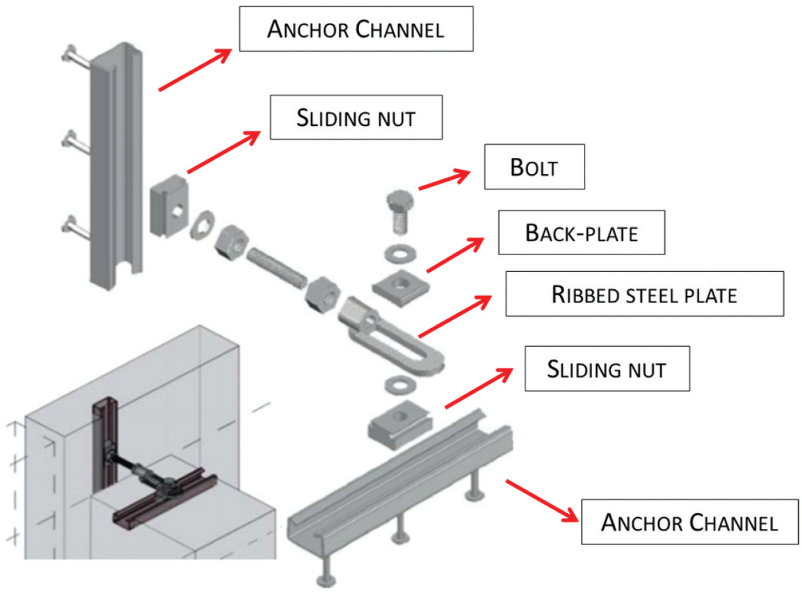

Figure 25. Connection device.

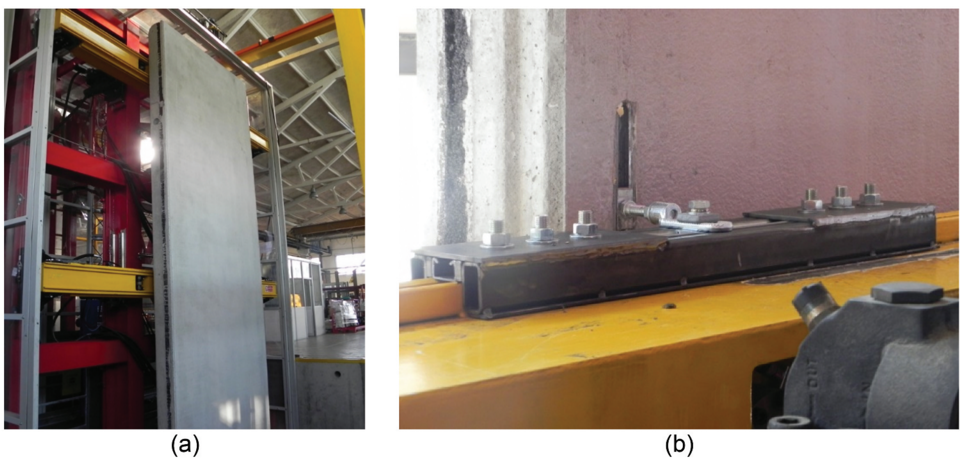

Figure 26. Experimental setup: (a) specimen; (c) connection detail.

As described in the previous section, the effective behaviour of the connection device under examination depends on its capacity to accommodate horizontal panel-to-structure in-plane displacements and to resist to the out-of-plane forces, at the same time. For this reason, at each level, the corresponding acceleration time-histories have been simultaneously applied to the specimen by means of two horizontal actuators in the out-of-plane direction and a horizontal actuator in the in-plane direction, fixed to the upper horizontal movable beam.

For tests No. 1 to 3 no significant damage has been observed. During the test No. 4, instead, the failure of the connection system occurred (i.e. the yielding of the steel bolt; Fig. 28), directly corresponding to the DS3 damage state.

The experimental results of the dynamic tests are presented in terms of:

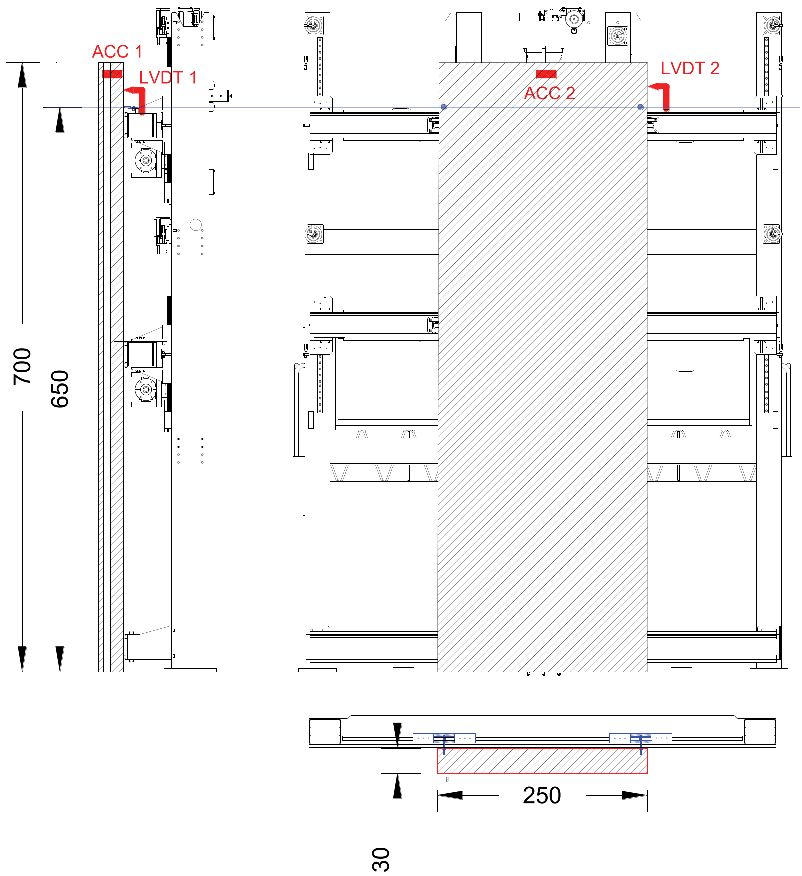

Figure 27. Panel layout and monitoring system layout.

Table 4. Loading steps.

	Scale factor for the reference time-history
Test No.1	0.25
Test No.2	0.50
Test No.3	0.75
Test No.4	1.00

(i) panel-to-beam mutual displacements, both in the in-plane (d^{IP} measured by LVDT 2 in Fig. 27) and out-of-plane (d^{OOP} measured by LVDT 1 in Fig. 27) direction;
(ii) in-plane and out-of-plane absolute accelerations at the head of the panel (a_p^{IP} and a_p^{OOP} measured by ACC 2 and ACC 1 in Fig. 27, respectively);

A bandpass filter has been applied to consider only the significant frequency range for the test specimen. Fig. 29 shows test results in terms of acceleration for tests No. 1 (left) and No. 4 (right), respectively. Fig. 30 shows test results in terms of mutual displacements, again for tests No. 1 (left) and No. 4 (right), respectively.

Considering that the current seismic requirements for non-structural components (Eurocode 8, CEN (2013) - §4.3.5.2 and §4.4.3.2) prescribe limit values in terms of interstory drift and out-of-plane floor acceleration, the peak values of d^{IP} and of a_p^{OOP} histories have been identified. Fig. 31 shows the d^{IP} history (black line) and the corresponding peak values

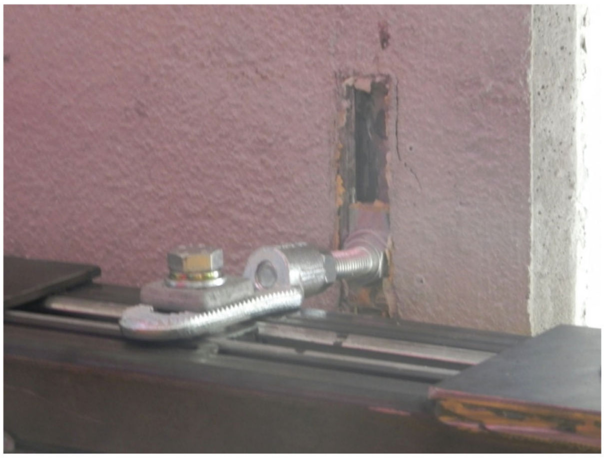

Figure 28. Failure of the connection system occurred for the test No. 4 (scale factor equal to 1.0).

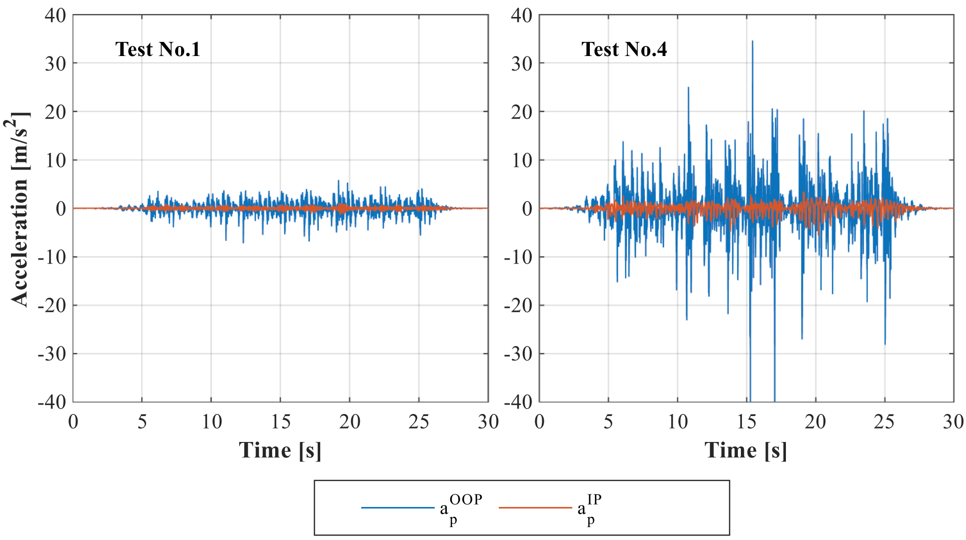

Figure 29. Test results in terms of acceleration.

$d^{IP,peak}$ (filled circles) for Test No. 1 (scale factor equal to 0.25). In the same figure, the empty circles represent the values of a_p^{OOP} corresponding to each $d^{IP,peak}$ $\left(\text{i.e.} a_p^{OOP}\left(d^{IP,peak}\right)\right)$. Similarly, Fig. 32 shows the a_p^{OOP} history (black line) and the corresponding peak values $a_p^{OOP,peak}$ (filled squares) for Test No. 1 (scale factor equal to 0.25). In the same figure, the empty squares represent the values of d^{IP} corresponding to each $a_p^{OOP,peak}$ $\left(\text{i.e.} d^{IP}\left(a_p^{OOP,peak}\right)\right)$. To make the graph easier to read, test results are represented only in the time frame 15–20 s. With the aim of approaching the definition of a displacement-acceleration interaction domain, which, as mentioned earlier, is considered the most appropriate tool for representing the seismic capacity of the connections under examination, all peak values (roughly, all circles in Fig. 31 and all squares in Fig. 32) are collected on a Cartesian plane where the abscissa

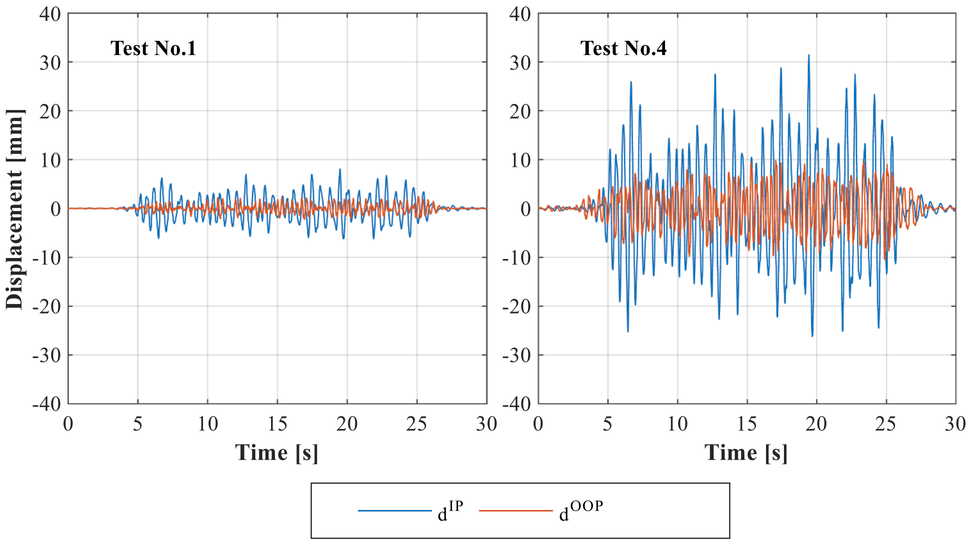

Figure 30. Peak values of d^{IP} and corresponding a_p^{OOP}, for test No. 1 (25%).

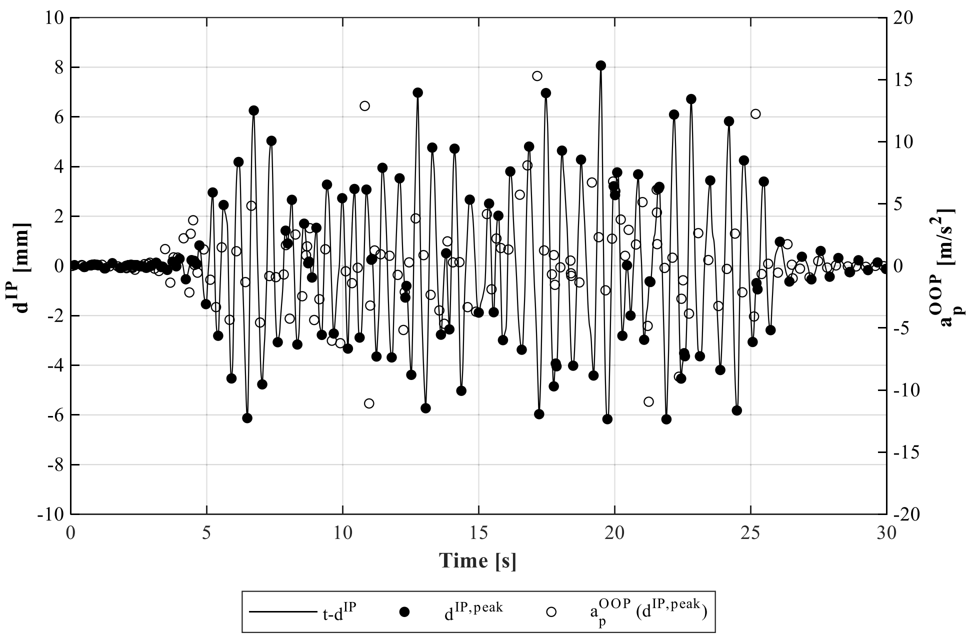

Figure 31. Peak values of d^{IP} and corresponding a_p^{OOP}, for test No. 1 (scale factor equal to 0.25).

represents the in-plane displacements and the ordinate represents the corresponding out-of-plane acceleration values (Fig. 33).

Fig. 33 shows that the experimental data correspond to a cloud of points that can be bounded by a convex domain. An ellipse is adopted as a typical shape for capacity domains. The ellipse that tightly circumscribes the points can be analytically described following the steps listed below:

(1) calculation of the abscissa and ordinate of the centroid as the mean value of the abscissas and ordinates of all the points, respectively;

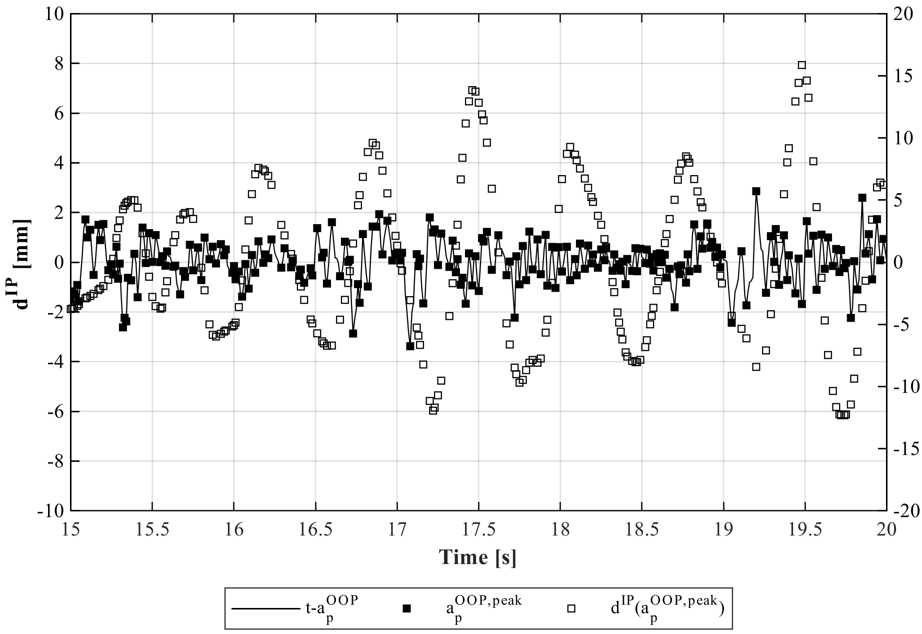

Figure 32. Peak values in term of a_p^{OOP} and corresponding d^{IP}, for test No. 1 (scale factor equal to 0.25).

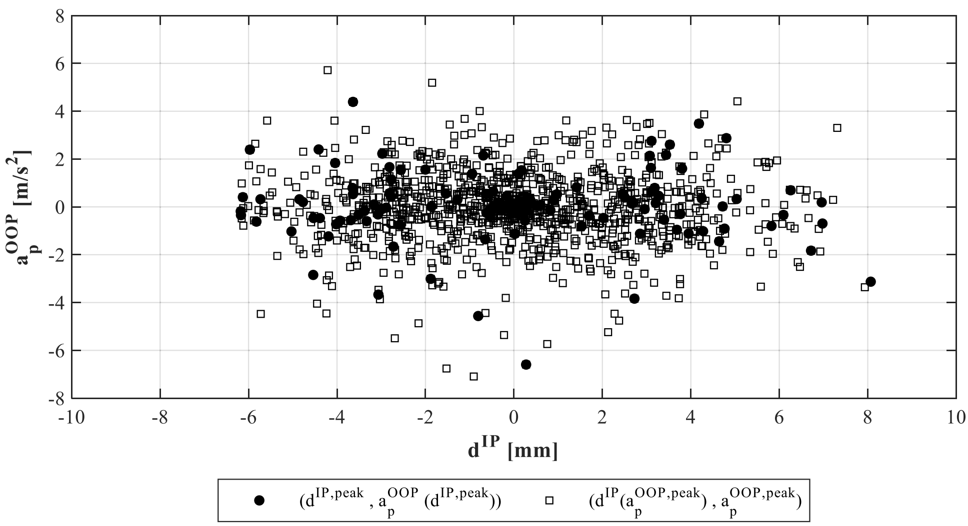

Figure 33. Peak values in term of d^{IP} and a_p^{OOP}, for test No. 1 (scale factor equal to 0.25).

(2) calculation of the radii of the ellipse, that is the horizontal, R_h, and the vertical, R_v, as mean value of the 1% and 99% quantiles respectively of the abscissas ($d_{1\%}^{IP}, d_{99\%}^{IP}$) and ordinates ($a_{p,1\%}^{OOP}, a_{p,99\%}^{OOP}$) of all the points (Eq. 3).

$$R_h = mean\left(|d_{1\%}^{IP}|, |d_{99\%}^{IP}|\right)$$
$$R_v = mean\left(\left|a_{p,1\%}^{OOP}\right|, \left|a_{p,99\%}^{OOP}\right|\right) \tag{3}$$

In the following, as an example, the construction of the ellipse for Test No. 1 (scale factor equal to 0.25) is shown. The centroid C of the ellipse (red diamond in Fig. 35) results to have

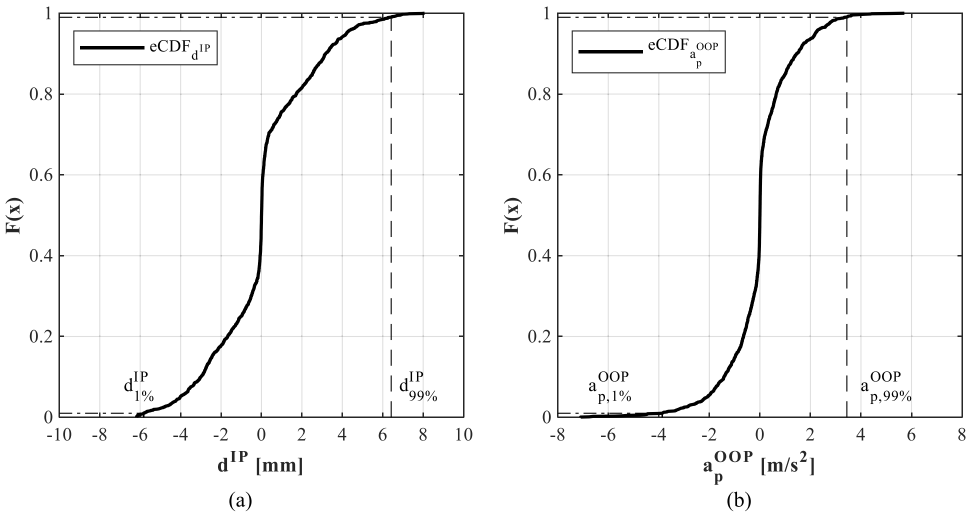

Figure 34. Empirical cumulative distribution functions of d^{IP}(a) and a_p^{OOP} (b) values, for test No. 1 (scale factor equal to 0.25).

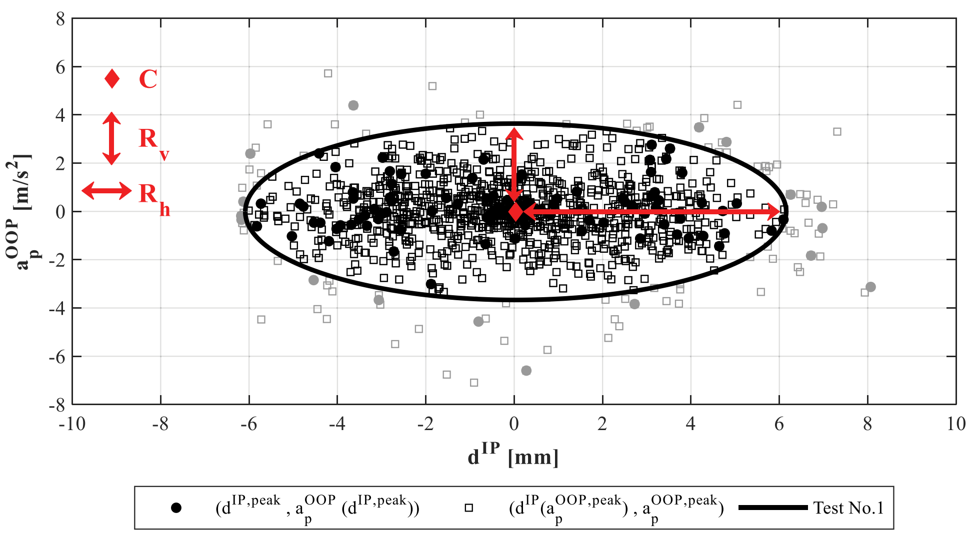

Figure 35. Ellipse representation for test No.1 (scale factor equal to 0.25).

abscissa, d_C^{IP},and ordinate, a_C^{OOP}, of 0.35 mm and −0.02 m/s^2, respectively. In accordance with Fig. 34, the reference quantiles for calculating the radii of the ellipse are ($d_{1\%}^{IP}$, $d_{99\%}^{IP}$) = (−5.82, 6.42) mm, yielding R_h = 6.12 mm, and ($a_{p,1\%}^{OOP}$, $a_{p,99\%}^{OOP}$)=(−3.86, 3.44) m/s^2, yielding R_v = 3.65 m/s^2. Fig. 35 shows the ellipse with determined as described above. Such steps have been repeated for tests No. 2, No. 3, and No. 4 (Figs. 36 and 37, Table 5).

The idea proposed in this paper is to draw an ellipse representing the envelope of the seismic demand corresponding to each of the dynamic analyses in the in-plane displacement – out-of-plane acceleration layer. Then, for each test – and thus each “ellipse” – to note the level of damage, if any, that was observed (DS1, DS2, DS3).

For sake of safety, the proposed method assumes the following definitions:

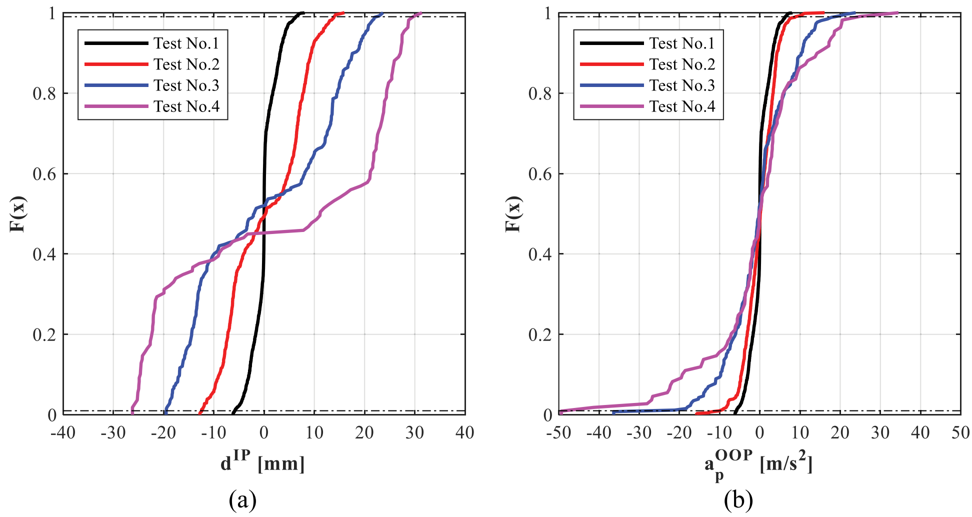

Figure 36. Empirical cumulative distribution functions of d^{IP}(a) and a_p^{OOP}(b) values, for all the tests.

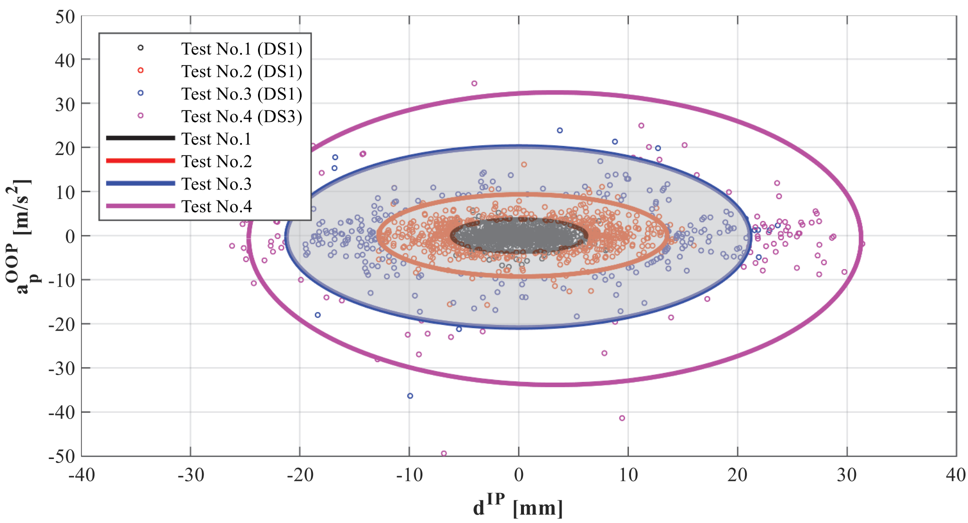

Figure 37. Ellipse representation in terms of d^{IP} and $a_p{}^{OOP}$ for all the tests.

Table 5. Statistical and geometrical characterization of the "envelope" ellipse for each of the 4 tests.

Test No.	Scale factor	$d^{IP}_{1\%}$ [mm]	$d^{IP}_{99\%}$ [mm]	$a^{OOP}_{p,1\%}$ [m/s^2]	$a^{OOP}_{p,99\%}$ [m/s^2]	d^{IP}_c [mm]	a^{OOP}_c [m/s^2]	R_h [mm]	R_v [m/s^2]
1	0.25	−5.82	6.42	−3.86	3.44	**0.35**	**−0.02**	**6.12**	**3.65**
2	0.50	−12.43	13.94	−9.70	8.91	**0.38**	**0.04**	**13.18**	**9.31**
3	0.75	−19.44	22.92	−21.20	19.82	**−0.04**	**0.33**	**21.18**	**20.51**
4	1.00	−26.20	29.75	−41.36	24.94	**3.31**	**−0.69**	**27.98**	**33.15**

- the safe region, which includes points whose coordinates correspond to solicitations that do not cause damage to the component, is the largest of the ellipses labelled with DS1 (i.e. operational, no damage);
- the boundary of the ellipse mentioned in the previous point constitutes the locus of the limit conditions between DS1 and DS2;
- similarly, the largest of the ellipses labelled with DS2 (life safety limit state) is considered the locus of the limit conditions between DS2 and DS3 (collapse prevention limit state).

In the case under examination, no damage was recorded for the first three tests, whereas a severe damage (DS3) has occurred during the test No. 4 (collapse of both connection devices), so the grey area in Fig. 37 represents the safe region against DS3.

In order to obtain a conservative representation of the capacity domains at each damage state for the connection system, in term of out-of-plane forces and in-plane panel-to-beam displacements, it is assumed that the resulting out-of-plane force at the top of the panel, neglecting any source of damping, corresponds to the sum of the inertial F_{in}^{OOP} and elastic F_{el}^{OOP} forces. These forces were obtained considering an effective mass m^* and an effective flexural stiffness k^*, respectively, according to the following assumptions and considering that two symmetrically connectors are installed (total force divided by two):

- considering the bottom and top panel constrains described in Section 5.2, a cantilever static scheme is adopted in the out-of-plane direction. The cantilever is excited according the first vibrational mode so that the equivalent modal mass m^* can be assumed equal to roughly one third of the total mass of the panel (6.3/3 = 2.1 Mg);
- considering that no damage was recorded in the connection devices at the bottom of the panel during the tests, a fixed constraint can be assumed so that the flexural stiffness k^* is that of a cantilever beam, that is $3EI/h_c^3$, where E is the concrete Young modulus (30 GPa), I the moment of inertia of the panel cross section and h_c the height of the installation point of the connectors to the base (6.5 m). The non-structural component at hand is a "sandwich" wall panel with two external concrete layer each 5.5 cm thick, whereas the panel width b is equal to 2.5 m, yielding for k^* *the value* 1,375 kN/m.

The resulting global out-of-plane force into the two devices, F^{OOP}, is therefore that in Eq. (4), while that acting on the single connector is half of it ($F_{conn}^{OOP}=F^{OOP}/2$).

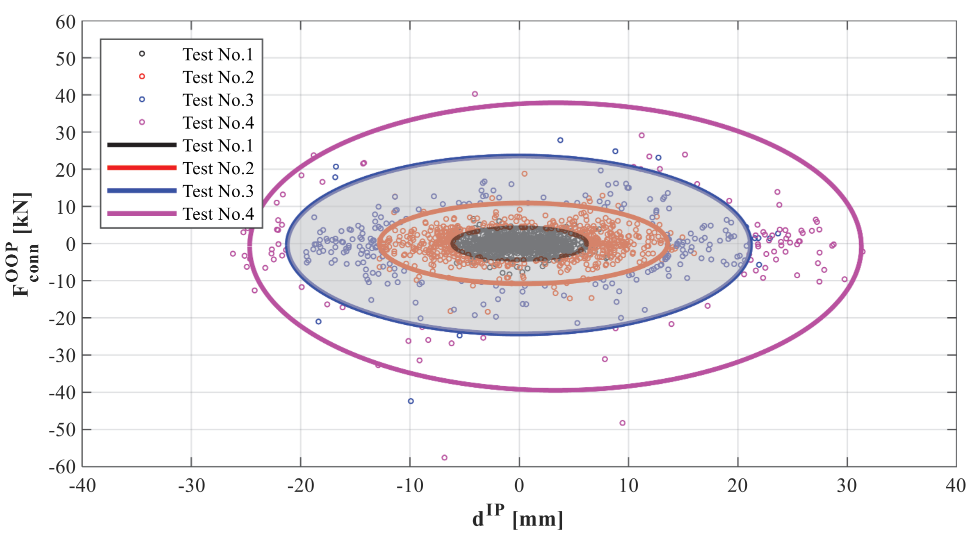

Figure 38. Ellipse representation in terms of d^{IP} and F_{conn}^{OOP} for all the tests.

$$F^{OOP} = F_{in}^{OOP} + F_{el}^{OOP} = m^* \cdot a_p^{OOP} + k^* \cdot d_{p,el}^{OOP} \tag{4}$$

in which $d_{p,el}^{OOP}$ represents the top-to-base displacement of the panel. Fig. 38 shows the ellipses assessed above, now reprocessed so as to have as ordinates the forces referred to the single connector, rather than the accelerations.

6. Conclusions and Future Perspectives

Seismic design of building envelopes requires specialized methodologies for the evaluation of seismic demand and for the assessment of seismic capacity of such non-structural components. For building envelopes, the evaluation of seismic demand is mainly based on floor response spectra, whereas the assessment of seismic capacity is generally determined through experimental activities. However, most of the studies on seismic capacity of non-structural components are based on the idea of adopting a testing equipment constructed for structural components to their non-structural counterpart. Even if this methodology can be successfully applied in some cases, the assessment of seismic capacity of building envelopes requires a specialized equipment. From these considerations, this paper describes:

- a specialized equipment purposefully designed and constructed to assess the seismic capacity of building envelopes or of their most significant components; the equipment can handle the testing needs for both acceleration sensitive and interstory-drift sensitive components, for both quasi-static and dynamic actions and for both in-plane and out-of-plane actions, also simultaneously;
- a companion testing protocol, based on recent design codes for nonstructural components, which fully exploits the capability of the testing equipment described above;
- the complete match between the components of the "testing set," namely the equipment and the protocol;
- a first application of the testing set to external wall cladding systems, based on out-of-plane dynamic and in-plane quasi-static tests;
- a second application of the testing set to specialized connections between precast concrete panels and pre-cast concrete structures, which, in turn, led to the definition of a new design criterium for such connections.

The above mentioned case studies highlight how the proposed methodology is robust for non-structural envelope systems and components that are very different from each other.

Hence, the demand can be translated into spectrum compatible seismic actions, both in-plane and out-of-plane directions, thanks to the special equipment created. On the other hand, the capacities are determined based on defined progressive damage states which are fixed according to the specific non-structural systems or element and its essential characteristics.

The damages can be assessed in terms of global mechanical response, as in case of external cladding mechanically fixed, or mechanical response of individual parts, as in the case of the connection system for precast panels. It is also possible to fix the damage in terms of thermo-hygrometric performance loss (air permeability and water tightness of the envelope system) or even in economic terms (refurbishment costs).

In this perspective future research activities will include the contextualization and use of this innovative testing set to different types of building envelopes and to their specialized components. Furthermore, the testing protocol will be further enhanced to include the check of serviceability conditions before and after the seismic tests, exploiting the additional capability of the testing apparatus in terms of resistance against wind pressure, static and dynamic water-tightness and air leakage.

Disclosure Statement

No potential conflict of interest was reported by the author(s).

Funding

This study has been developed in the framework of the DPC-ReLUIS Agreement 2024-2026, WP17 "*Non-structural elements*", funded by the Italian Department of Civil Protection (DPC). This support is gratefully acknowledged.

Data Availability Statement

The authors confirm that the data supporting the findings of this study are available on request from the corresponding author, [C. O.], upon reasonable request.

References

AAMA 501.6. 2001. *Recommended Dynamic Test Method for Determining the Seismic Drift Causing Glass Fallout from Window Wall, Curtain Wall and Storefront Systems*. Schaumburg, Illinois: American Architectural Manufacturers Association.

Aghababaei, M., C. Okamoto, M. Koliou, T. Nagae, C. P. Pantelides, K. L. Ryan, A. R. Barbosa, S. Pei, J. W. van de Lindt, and S. Dashti. 2021. "Full-Scale Shake Table Test Damage Data Collection Using Terrestrial Laser-Scanning Techniques." *Journal of Structural Engineering – ASCE* 147 (3). https://doi.org/10.1061/(ASCE)ST.1943-541X.0002905.

Bedon, C., A. Xihong, F. Santos, D. Honfi, M. Kozloski, M. Arrioni, L. Figuli, and D. Lange. 2018. "Performance of Structural Glass façades Under Extreme Loads – Design Methods, Existing Research, Current Issues and Trends." *Construction and Building Materials* 163 (2018): 921–937. https://doi.org/10.1016/j.conbuildmat.2017.12.153.

Behr, R. A., A. Belarbi, and A. T. Brown. 1995. "Seismic Performance of Architectural Glass in a Storefront Wall System." *Earthquake Spectra* 11 (3): 367–391. https://doi.org/10.1193/1.1585819.

Behr, R., and A. Belarbi. 1996. "Seismic Test Methods for Architectural Glass Systems." *Earthquake Spectra* 12 (1): 129–143. https://doi.org/10.1193/1.1585871.

Bianchi, S., C. Andriotis, T. Klein, and M. Overend. 2024. "Multi-Criteria Design Methods in façade Engineering: State-Of-The-Art and Future Trends." *Building & Environment* 250 (2024): 111184. https://doi.org/10.1016/j.buildenv.2024.111184.

Bianchi, S., and S. Pampanin. 2022. "Fragility Functions for Architectural Nonstructural Components." *ASCE Journal of Structural Engineering* 148 (10). https://doi.org/10.1061/(ASCE)ST.1943-541X.0003352.

Bouwkamp, J. 1960. Behavior of Window Panels Under In-Plane Forces. *UCB/SESM Report 1960/06*. Berkeley, CA: University of California.

Bouwkamp, J., and J. Meehan. 1960. "Drift Limitations Imposed by Glass." Proc. of the Second World Conference on Earthquake Engineering (2WCEE), Tokyo, Japan, 1763-78.

Brueggeman, J. L., R. A. Behr, H. Wulfert, A. M. Memari, and P. A. Kremer. 2000. "Dynamic Racking Performance of an Earthquake-Isolated Curtain Wall System." *Earthquake Spectra* 16 (4): 735–756. https://doi.org/10.1193/1.1586137.

CEN, EN 13830:2003. 2003. *Curtain Walling – Product Standard, Performance Requirements*. Brussels: European Committee for Standardization.

CEN, EN 13830:2015. 2015. *Curtain Walling – Product Standard, Performance Requirements*. Brussels: European Committee for Standardization.

CEN, EN 13830:2022. 2022. *Curtain Walling – Product Standard, Performance Requirements*. Brussels: European Committee for Standardization.

CEN, EN 1998-1:2004/A1:2013. 2013. *Eurocode 8: Design of Structures for Earthquake Resistance - Part 1: General Rules, Seismic Actions and Rules for Buildings*. Brussels: European Committee for Standardization.

Culp, J. H. 1993. "In-Plane/out-Of-Plane Dynamic Racking Tests of Curtain Wall Glass Elements, Opportunities for Undergraduate Research Experience Program (OURE)." (79). https://scholarsmine.mst.edu/oure/79.

D'Angela, D., G. Magliulo, C. Di Salvatore, and M. Zito. 2024. "Seismic Assessment and Qualification of Acceleration-Sensitive Nonstructural Elements Through Shake Table Testing: Reliability of Testing Protocols and Reliability-Targeted Safety Factors." *Engineering Structures* 301:117271. https://doi.org/10.1016/j.engstruct.2023.117271.

Deschenes, J. P. 1991. "Dynamic Racking Performance of Curtain Wall Glass Elements." Masters Thesis No. 1031, University of Missouri-Rolla. https://scholarsmine.mst.edu/masters_theses/1031.

Deschenes, J. P., R. A. Behr, C. P. Pantelides, and J. E. Minor. 1991. *Dynamic Racking Performance of Curtain Wall Glass Elements*. University of Missouri - Rolla: Building Envelope Research Laboratory, University of Missouri-Rolla.

EOTA. 2021. "EAD 090062-01-0404, Kit for External Wall Claddings Mechanically Fixed." OJ Publication: Decision (EU) 2024/237.

FEMA 461. 2007. *FEMA, Interim Protocols for Determining Seismic Performance Characteristics of Structural and Nonstructural Components Through Laboratory Testing*, Report No. Washington DC: Federal Emergency Management Agency (FEMA).

Fiorino, L., S. Shakeel, A. Campiche, and R. Landolfo. 2023. "In-Plane Seismic Behavior of Lightweight Steel Drywall façades Through Quasi-Static Reversed Cyclic Tests." *Thin-Walled Structures* 182 (2023): 110157. https://doi.org/10.1016/j.tws.2022.110157.

Hancock, J., J. Watson-Lamprey, N. A. Abrahamson, J. J. Bommer, A. Markatis, E. M. M. A. McCoy, and R. Mendis. 2006. "An Improved Method of Matching Response Spectra of Recorded Earthquake Ground Motion Using Wavelets." *Journal of Earthquake Engineering* 10 (sup001): 67–89. https://doi.org/10.1080/13632460609350629.

Huang, B., W. Lu, S. Chen, and K. M. Mosalam. 2017. "Drift Demand of the Outer-Skin Curtain Wall System of the Shangai Tower, Structural Design of Tall and Special Buildings." *The Structural Design of Tall & Special Buildings* 26 (17): 31388. https://doi.org/10.1002/tal.1388.

ICC-ES (International Code Council Evaluation Service). 2020. *AC156 Acceptance Criteria for the Seismic Certification by Shake-Table Testing of Nonstructural Components*. Brea, California, USA: International Code Council.

Kazantzi, A. K., D. Vamvatsikos, and E. Miranda. 2020. "Evaluation of Seismic Acceleration Demands on Buildings Nonstructural Elements." *Journal of Structural Engineering – ASCE* 146 (7): 04020118–1 to 10. https://doi.org/10.1061/(ASCE)ST.1943-541X.0002676.

Magliulo, G., V. Pentangelo, G. Maddaloni, V. Capozzi, C. Petrone, P. Lopez, R. Talamonti, and G. Manfredi. 2012. "Shake Table Tests for Seismic Assessment of Suspended Continuous Ceilings." *Bulletin of Earthquake Engineering* 10 (6): 1819–1832. https://doi.org/10.1007/s10518-012-9383-6.

Medina, R. A., R. Sankaranarayanan, and K. M. Kingston. 2006. "Floor Response Spectra for Light Components Mounted on Regular Moment-Resisting Frame Structures." *Engineering Structures* 28 (14): 1927–1940. https://doi.org/10.1016/j.engstruct.2006.03.022.

Merino, R. J., D. Perrone, and A. Filiatrault. 2022. "Appraisal of Seismic Design Methodologies for Suspended Non-Structural Elements in Europe." *Bulletin of Earthquake Engineering* 20 (15): 8061–8098. https://doi.org/10.1007/s10518-022-01492-y.

Mulligan, J. G., T. J. Sullivan, and R. P. Dhakal. 2020. "Experimental Study of the Seismic Performance of Plasterboard Partition Walls with Seismic Gaps." *Bulletin of the New Zealand Society for Earthquake Engineering* 53 (4): 175–188. December 2020. https://doi.org/10.5459/bnzsee.53.4.175-188.

Oropeza, M., P. Favez, and P. Lestuzzi. 2010. "Seismic Response of Nonstructural Components in Case of Nonlinear Structures Based on Floor Response Spectra Method." *Bulletin of Earthquake Engineering* 8 (2): 387–400. https://doi.org/10.1007/s10518-009-9139-0.

Pantelides, C. P., and R. A. Behr. 1994. "Dynamic In-Plane Racking Tests of Curtain Wall Glass Elements." *Earthquake Engineering & Structural Dynamics* 23 (2): 211–228. https://doi.org/10.1002/eqe.4290230208.

Pourali, A., R. P. Dhakal, G. MacRae, and A. S. Tasligedikc. 2017. "Fully Floating Suspended Ceiling System: Experimental Evaluation of Structural Feasibility and Challenges." *Earthquake Spectra* 33 (4): 1627–1654. https://doi.org/10.1193/092916eqs163m.

Taghavi, S., and E. Miranda. 2003. Response Assessment of Nonstructural Building Elements, Pacific Earthquake Engineering Research. *Center Report 2003/05*. University of California Berkeley.

Thurston, S. J., and A. B. King. 1992. Two-Directional Cyclic Racking of Comer Curtain Wall Glazing, Building Research Association of New Zealand, Study Report SR 44. Judgeford, New Zealand.

Villaverde, R. 2006. "Simple Method to Estimate the Seismic Nonlinear Response of Nonstructural Components in Buildings." *Engineering Structures* 28 (8): 1209–1221. https://doi.org/10.1016/j.engstruct.2005.11.016.

Wynn, S., K. L. Ryan, W. Roser, I. Ji, S. Sorosh, and T. C. Hutchinson. 2022. "NHERI TallWood 10-Story Test Nonstructural, Part 1 of 4: Project Overview and Curtain Wall Subassembly." Proceedings of the 12th National Conference in Earthquake Engineering, Earthquake Engineering Research Institute, Salt Lake City, UT.

Zito, M., D. D'Angela, G. Maddaloni, and G. Magliulo. 2022. "A Shake Table Protocol for Seismic Assessment and Qualification of Acceleration-Sensitive Nonstructural Elements." *Computer-Aided Civil and Infrastructure Engineering* 38 (12): 1699–1726. https://doi.org/10.1111/mice.12951.

Zito, M., R. Nascimbene, P. Dubini, D. D'Angela, and G. Magliulo. 2022. "Experimental Seismic Assessment of Nonstructural Elements: Testing Protocols and Novel Perspectives." *Buildings* 12 (11): 1871. https://doi.org/10.3390/buildings12111871.